

Modeling and Simulating Human Cardiovascular Response to Acceleration

by

Sam Ahmad Zamanian

B.S., Johns Hopkins University (2005)

Submitted to the Department of Electrical Engineering and Computer Science
in partial fulfillment of the requirements for the degree of

Master of Science

at the

MASSACHUSETTS INSTITUTE OF TECHNOLOGY

June 2007

© Massachusetts Institute of Technology, MMVII. All rights reserved.

Author _____
Department of Electrical Engineering and Computer Science
May 25, 2007

Certified by _____

George C. Verghese
Professor of Electrical Engineering
Thesis Supervisor

Certified by _____

Thomas Heldt
Postdoctoral Associate
Thesis Supervisor

Accepted by _____

Arthur C. Smith
Chairman, Department Committee on Graduate Students

MASSACHUSETTS INSTITUTE
OF TECHNOLOGY

AUG 16 2007

LIRRARIES

ARCHIVES

In the Name of Allah,

To my parents, Ahmad and Farideh.

**Modeling and Simulating Human Cardiovascular Response to
Acceleration**

by
Sam Ahmad Zamanian

Submitted to the Department of Electrical Engineering and Computer Science
on May 25, 2007, in partial fulfillment of the
requirements for the degree of
Master of Science

Abstract

The human cardiovascular system routinely encounters conditions that cause it to adapt. For example, when an astronaut enters microgravity, his/her cardiovascular system adapts rapidly to the weightless environment with no functional impairment. This adaptation is entirely appropriate while in space. However, it predisposes astronauts to problems when they return. It has been suggested that the regimen for astronauts on long-duration space travel include periods of artificial acceleration via centrifugation, in order to maintain some exposure to a gravitational gradient and thus ameliorate some of the physiological consequences of exposure to microgravity. To design such an intervention, it is desirable to know and understand, as well as to predict the cardiovascular response to centrifugation stress. A reasonably compartmentalized mathematical model of the cardiovascular system that represents these conditions is presented, which will allow for understanding and predicting cardiovascular behavior under such conditions. We validated our simulations against human data and showed that our results closely matched the experimental data. Upon validation, we used our model to predict the response of the cardiovascular system to levels of stress that cannot yet be tested on human subjects.

Thesis Supervisor: George C. Verghese
Title: Professor of Electrical Engineering

Thesis Supervisor: Thomas Heldt
Title: Postdoctoral Associate

Acknowledgements

I begin by thanking my Creator, Allah, to Whom is due all praise and thanks and Who granted me the ability to do this work.

I would like to thank Professor George Verghese, my thesis advisor, for his support and guidance throughout my time at MIT. His insight and wisdom have been invaluable to my research. I can honestly say that George went above and beyond the role of a typical advisor, showing concern and support for all his students beyond the scope of academics. Thank you George for your mentorship, which has inspired the intellectual curiosity for me to continue my studies.

I would also like to thank Dr. Thomas Heldt who has played a very active role in the supervision of my work. Many are the days I would spend working right outside Thomas's office, constantly entering, and receiving new insight and advice with each entry. His extensive knowledge of both physiology and engineering have greatly aided my work. I would also like to thank Professor Roger Mark for overseeing and supporting this work.

I would like to thank the entire Laboratory for Electromagnetic and Electronic Systems, and, in particular, the Cardiovascular Modeling Group for their companionship, moral support, and humor. Perhaps it is the camaraderie of colleagues and the understanding that others are also subject to the same (if not higher) intensity of work that allows a student to exert himself beyond his limits. In particular, I would like to thank Faisal Kashif, not only for his friendship, humor, excellent Pakistani food, and even housing, but also for proofreading and reviewing the final chapters of my thesis. I would also like to thank Tushar Parlikar for his friendship and general help with different aspects of graduate student life.

A special thanks goes to Hanif Khalak, Saeed Amin, Tariq Mehenna, Tauqeer Zaidi, Umair Ahsun, Imam Suheil Laher, Anas Ahsan, and many others who have gone unmentioned, for their friendship, brotherhood, support, and personal and religious guidance.

They have made my short stay in Boston a truly memorable one. I also owe a great deal of gratitude to Danial Lashkari, Ali Shoeb, and Tarek El Moselhy, who, besides their kind friendship, have all, at some point or other at MIT, assisted me with my studies. Also, I could never forget my close friends from my undergraduate years, namely Safiullah Shareef, Nabil Rab, Sameer Ahmed, Darryn Nasir Jones, and AbdulRasheed Alabi, amongst many others, who have been excellent friends and brothers and have supported me throughout our friendship.

Finally, I move on to thanking those dearest and closest to me. My father, Ahmad, you have been a true source of inspiration in my life; I cannot thank you enough for your love, support, and discipline. I still look to you as a role-model and mentor, both as a person and as an engineer. My mother, Farideh, it is you who nurtured me, cared for me, and supported me throughout my life; I would not be the same person without your support and am ever grateful for all you have done for me. Again, I cannot thank the both of you enough, and I would like to dedicate this thesis to you, my dear parents. I also express much thanks to my sisters, Neeki and Donna, for their warm friendship and support.

And now I come to the one who perhaps has been the most burdened by my graduate studies, more so than even myself, and that is my wonderful wife Sabah. I cannot possibly express how grateful I am for your love, support, and patience during this chapter of our life. I thank you for putting up with my busy schedule and the numerous all-nighters I had to pull in order to complete my work. May Allah reward you immensely for your patience and support. I would also like to thank my father-in-law, Chiragh Chaudhry, my mother-in-law, Zahida Chaudhry, my brothers-in-law, Ahmed and Daniel, and my sisters-in-law, Farah and Ammara, for their kindness and support.

This work was supported in part by the National Aeronautics and Space Administration (NASA) through the NASA Cooperative Agreement NCC 9-58 with the National Space Biomedical Research Institute and in part by grant R01 EB001659 from the National Institute of Biomedical Imaging and Bioengineering of the United States Institutes of Health.

Contents

1	Introduction	13
1.1	Motivation	13
1.2	Background	14
1.2.1	The Cardiovascular System	14
1.2.2	Cardiovascular Models	14
1.3	Thesis Organization	16
2	Hemodynamic Model	17
2.1	Choice of a Proper Model	18
2.2	Systemic Circulation	19
2.2.1	Non-linearities	22
2.3	Cardiopulmonary Circulation	24
2.3.1	Cardiac Compartments	24
2.3.2	Pulmonary Circulation	26
2.3.3	Cardiac Pacemaker	27
2.4	Modeling Orthostatic Stress	28
2.4.1	Upright Tilt	29
2.4.2	Lower Body Negative Pressure	31
2.4.3	Centrifugation	32
2.5	Modeling Vessel Collapse	34
2.5.1	Pressure-Volume Relationship	35
2.5.2	The Starling Resistor	37
2.5.3	Volume-Dependent Resistance	38
2.6	Model Implementation	41
2.6.1	Platform	41
2.6.2	Choice of State Variables	41
2.6.3	Integration Routine	43
2.6.4	Initial Conditions	44
2.7	Concluding Remarks	44
3	The Cardiovascular Control System	47

Contents

3.1	Arterial Baroreflex	49
3.1.1	Architecture	49
3.2	Cardiopulmonary Reflex	52
3.3	Implementation	53
4	Model Validation and Prediction	55
4.1	Data Acquisition	55
4.2	Model Validation	56
4.3	Prediction with Centrifugation Simulations	62
4.4	Summary	65
5	Conclusions and Recommendations for Future Work	67
5.1	Summary	67
5.2	Recommendations for Future Work	69
A	Analytical Solutions to Interstitial Fluid Flow and Volume	71
B	Method for Finding Initial Conditions to Hemodynamic Model	73
C	Description of Simulink and MATLAB Code for the Cardiovascular Model	77
D	Data Processing Code	91
	Bibliography	95

List of Figures

2.1	Circuit representation of a vascular compartment.	18
2.2	Circiut representation of Heldt's model.	20
2.3	Circuit representation of atrial and ventricular cardiac compartments.	25
2.4	RC model of interstitial compartment.	30
2.5	Pressure-volume relation of a common iliac vein.	36
2.6	Model for the Pressure-Volume Relation for a Collapsible Vessel.	37
2.7	Model for Volume-Dependent Resistance for a Collapsible Vessel.	40
2.8	Change in total volume during a 100 $\frac{\text{rev}}{\text{min}}$ centrifugation simulation.	45
3.1	A block diagram representation of the cardiovascular control system.	48
3.2	A block diagram representation of the effector mechanism for autonomic mediation.	51
4.1	Comparison of simulation to data of transient changes in heart rate during centrifugation.	57
4.2	Comparison of simulation to data of transient changes in mean arterial pressure during centrifugation.	58
4.3	Comparison of simulation to data of transient changes in systolic arterial pressure during centrifugation.	59
4.4	Comparison of simulation to data of transient changes in diastolic arterial pressure during centrifugation.	60
4.5	Comparison of simulation to data of transient changes in leg volume during centrifugation.	61
4.6	Simulated response of blood volume in the upper-body and renal veins to centrifugation at a range of angular velocities.	62
4.7	Simulated response of mean arterial pressure, systolic arterial pressure, and diastolic arterial pressure to centrifugation at a range of angular velocities.	63
4.8	Simulated response of heart rate to centrifugation at a range of angular velocities.	64
4.9	Simulated response of blood volume in the legs to centrifugation at a range of angular velocities.	65
4.10	Simulated response of cardiac output, stroke volume, and total peripheral resistance to centrifugation at a range of angular velocities.	66
C.1	Schematic drawing for the layout of the code for the cardiovascular model. .	78

List of Figures

C.2 Actual Simulink code used for the cardiovascular model.	79
---	----

List of Tables

2.1	Parameter values for the systemic arterial compartments.	23
2.2	Parameter values for the systemic venous compartments.	24
2.3	Parameter values for the systemic microvascular resistances.	24
2.4	Cardiac Model Parameters.	25
2.5	Values for cardiac timing parameters.	26
2.6	Parameter values for pulmonary compartments.	27
2.7	Values for $R_i - d$	33
3.1	Parameterization of the sympathetic impulse response function.	50
3.2	Gain values for the arterial baroreflex model.	52
3.3	Gain values for the cardiopulmonary reflex model.	53
C.1	Corresponding model variables for outputs from code	81

Chapter 1

Introduction

1.1 Motivation

The human cardiovascular system routinely encounters conditions that cause it to adapt. For example, when an astronaut enters microgravity, his/her cardiovascular system adapts rapidly to the weightless environment with no functional impairment. This adaptation is entirely appropriate while in space. However, it predisposes astronauts to problems when they return. It has been suggested that the regimen for astronauts on long-duration space travel include periods of artificial acceleration via centrifugation, in order to maintain some exposure to a gravitational gradient and thus ameliorate some of the physiological consequences of exposure to microgravity. To design such an intervention, it is desirable to know and understand as well as predict the cardiovascular response to centrifugal stress. In the case of the application of a centrifugal accelerational field to astronauts, we would like to be able to predict the cardiovascular system's response as a function of centrifuge parameters (angular acceleration, angular velocity, duration of centrifugation). As the radial acceleration resulting from centrifugation is a direct function of the distance from the center of rotation (as opposed to gravitational acceleration, which is uniform), analyzing the response of the system to centrifugal acceleration will be greatly aided by detailed computation. In order to understand how the system is behaving and to predict cardiovascular behavior under such conditions, a model of the cardiovascular system that represents these conditions is desirable. Current models [1, 2] can be extended to account for the effects of such conditions. A reasonably compartmentalized model seems necessary to account for the pressure distribution resulting from centrifugal acceleration. The model should simulate both the

Introduction

transient system response as well as its cyclic steady-state response. The results of the model can be compared to experimental data, and, when coupled to parameter estimation schemes, model parameters can be estimated in order to arrive at a better understanding and prediction of cardiovascular behavior under acceleration stress.

1.2 Background

1.2.1 The Cardiovascular System

The human cardiovascular system pumps blood through a closed circulatory system in order to deliver oxygen and nutrients and remove metabolic waste products from tissue. The cardiovascular circulation involves the right heart, the pulmonary arteries, the pulmonary capillaries, the pulmonary veins, the left heart, the systemic arteries, the systemic capillaries, and the systemic veins. The right heart receives de-oxygenated blood from the systemic veins and pumps the blood into the pulmonary circulation, where oxygen from the lungs diffuses into the de-oxygenated blood through the thin capillary walls. The oxygenated blood is transported via the pulmonary veins to the left heart, which pumps the blood into the systemic arteries. The systemic arteries branch into smaller vessels carrying the blood to the various organs. The blood then reaches the systemic capillaries where oxygen, nutrients, and waste products are exchanged via diffusion across capillary walls. The de-oxygenated blood is then transported to the systemic veins, which carry it to the right heart to be again pumped into the pulmonary circulation.

1.2.2 Cardiovascular Models

The cardiovascular system can be modeled using an electrical circuit analog. As early as 1899, a first-order system modeling arterial dynamics as a mechanical system analog of a single capacitor-resistor network, called the Windkessel model, was employed by Otto Frank [3]. As computational resources became affordable, circuit-based models of car-

1.2 Background

diovascular function became more abundant and more complex. For example, a simple cardiovascular model called the cardiovascular simulator (CVSIM), originally developed by Jah, Moody, and Davis at MIT as an aid to teaching cardiovascular physiology, divides the cardiovascular system into six compartments (left heart, right heart, pulmonary arteries, pulmonary veins, systemic arteries, and systemic veins) [1]. A more complex model by Heldt [2] accounts for the compartmental nature of the systemic circulation, which is divided into 15 compartments (as opposed to only two in Davis's model). Heldt's model also consists of control loops for the arterial baroreceptor and cardiopulmonary reflex. In 1993 Sud et al. [4] employed a 264-node finite-element method modeling the human cardiovascular system as an arrangement of many interconnected circulatory branches. The effects of lower-body negative pressure (LBNP) on the distribution of blood flow was simulated by lowering the external pressure in the lower extremities of the model. Likewise, in a paper published in 1994, Melchior et al. [5] modeled LBNP by considering individually its effects on (1) blood volume redistribution, (2) left ventricular end-diastolic filling, (3) the interaction between the left ventricle and peripheral circulation, and (4) the modulations of peripheral resistances and heart rate by arterial baroreceptor and cardiopulmonary reflexes, then combining the effects on the various model elements to model LBNP's overall effects on the cardiovascular system. Several models representing the effects of various gravitational loads (G-loads) on the cardiovascular system have been published, for instance by Jaron et al. [6] and Green et al. [7]. In the way of modeling the effects of centrifugation, Pancratz and colleagues developed a hemodynamic model capable of representing the G-gradient across the body resulting from centrifugation [8].

Experimental Studies According to short-radius centrifugation experiments (with the center of rotation located just above the head of the human subject) conducted by Young et al. [9] in the Man-Vehicle Lab at MIT, as the angular velocity of the centrifuge was increased from 0 to 23 revolutions per minute (rpm) over a 23 s period, the average heart rate of the subjects was significantly elevated from 70 to 76 beats per minute (bpm). However, no differences were found in heart rate between the stationary phase, while rotating at a

Introduction

constant velocity of 23 rpm (after reaching steady state), or after the experiment had ended. Hastreiter and Young conducted a similar study where they showed that the cardiovascular responses to short-radius centrifugation with 1.5 G at the feet were statistically similar to standing, the primary effects being an elevated diastolic pressure, increases heart rate, and increased calf volume [39].

1.3 Thesis Organization

Our primary objective in this thesis is to construct a model of the cardiovascular system that is capable of simulating and predicting the cardiovascular response to short-radius centrifugation. Such a model can then be employed in order to optimize the centrifugal stress test to best prevent cardiovascular deconditioning.

In Chapter 2, we detail the architecture and implementation of the computational (open-loop) hemodynamic model in which the framework for simulating the orthostatic stress resulting from centrifugation will be integrated. Chapter 3 focuses on the model for the cardiovascular control system which is integrated with the hemodynamic model.

In Chapter 4, we compare our simulations to experimental data in order to validate the model described in Chapters 2 and 3 and use our model to make predictions about the response of the cardiovascular system to a range of levels of centrifugation stress.

In Chapter 5, we conclude our work and suggest avenues for future research.

Chapter 2

Hemodynamic Model

The cardiovascular system, consisting of a regulated network of interconnected vessels and a pump (i.e. the heart), can be viewed as a fluidic system with regulatory control loops. Conveniently, fluidic systems can be represented as electric circuit analogs. The flow of blood (q , $\frac{\text{mL}}{\text{sec}}$) through a vessel impeded by resistance (R , $\frac{\text{mmHg}\cdot\text{s}}{\text{mL}}$, PRU) from vessel walls and driven by a pressure gradient (P , mm Hg) can be represented as the flow of charge through a resistive wire driven by a voltage gradient. Furthermore, the hydrostatic contribution to the pressure gradient resulting from orthostatic stress (P_h) can be modeled as a voltage source in series with the vessel. Since the vessel also stores blood volume (V , mL), it can be connected to a capacitor, where charge represents blood volume and capacitance represents compliance (C , $\frac{\text{mL}}{\text{mmHg}}$). Vessel compliance is the inverse of vessel elastance (E , $\frac{\text{mmHg}}{\text{mL}}$), which is a measure of vessel rigidity. Therefore, the volume stored in a vessel can be modeled as a function of the transmural pressure, which is the difference between the luminal pressure and the pressure external to the vessel (P_e). As the heart is a pump, its individual chambers can be modeled as vessels with time-varying elastances. In diastole, the heart has low elastance (i.e. high compliance), which allows it to store more blood volume for a given transmural pressure. During systole, the heart increases in elastance (and decreases in compliance) causing an increase in transmural pressure, which in turn causes heart volume to decrease and forces blood out of the heart. The heart valves, which ensure unidirectional flow, can be represented as diodes in the electric circuit analog. Figure 2.1 illustrates the electric circuit analog of a vascular compartment of the cardiovascular system. Thus, in the electric circuit analog, voltage represents pressure, current represents blood flow, charge represents blood volume, capacitance represents compliance, electric resistance represents fluidic resistance,

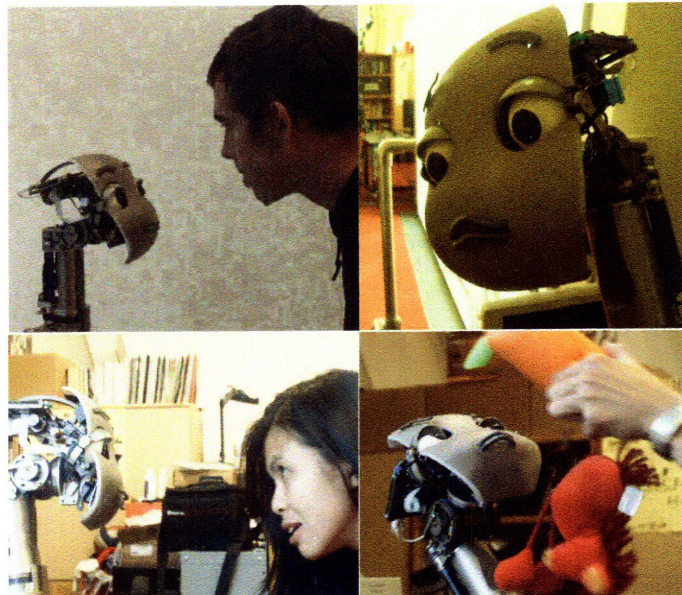


Figure 1-1: Mertz is an expressive head robot designed to explore incremental individual recognition through natural interaction. The robot's task is to learn to recognize a set of familiar individuals in an incremental and unsupervised fashion.

vessel in the circulation and doing so would be extremely tedious and impractical. Rather, we can work with a model that lumps together the various vessels that are found in each vertical component of the body in a physiologically meaningful manner. The portion of the cardiovascular system which circulates blood from the left heart to the various vertically distributed organs and back to the right heart is termed the systemic circulation. The systemic circulation consists of three main components: the arterial circulation, the microcirculation (consisting of the arterioles and capillaries), and the venous circulation.

We are then in search of a model that adequately compartmentalizes these three components of the systemic circulation along the vertical axis of the body. Heldt's model of the cardiovascular system [2] (introduced in Section 1.2.2) is reasonably complex and accounts for the compartmentalized nature of the systemic circulation, dividing the systemic circulation into 15 compartments. Figure 2.2 displays Heldt's model in its circuit representation. The model is comprised of a total 21 compartments: 15 for the systemic circulation, one compartment for each of the right atrium, left atrium, right ventricle, and left ventricle, and two compartments for the pulmonary circulation. We chose to employ Heldt's model of the cardiovascular system due to its reasonably compartmentalized nature which will readily allow us to model and simulate the response of the cardiovascular system to centrifugation and lower-body negative pressure (see Section 2.4). Appropriate modifications of Heldt's model will be described later in this chapter.

2.2 Systemic Circulation

Our model of the systemic circulation will follow Heldt's model without modification. The systemic circulation is modeled as 15 vascular compartments connected in series and parallel following the branching of the systemic circulation. Each vascular compartment is modeled as a circuit component as shown in Figure 2.1. The equations for the flows through each compartment are found by solving for the current through the resistors and capacitor in

Hemodynamic Model

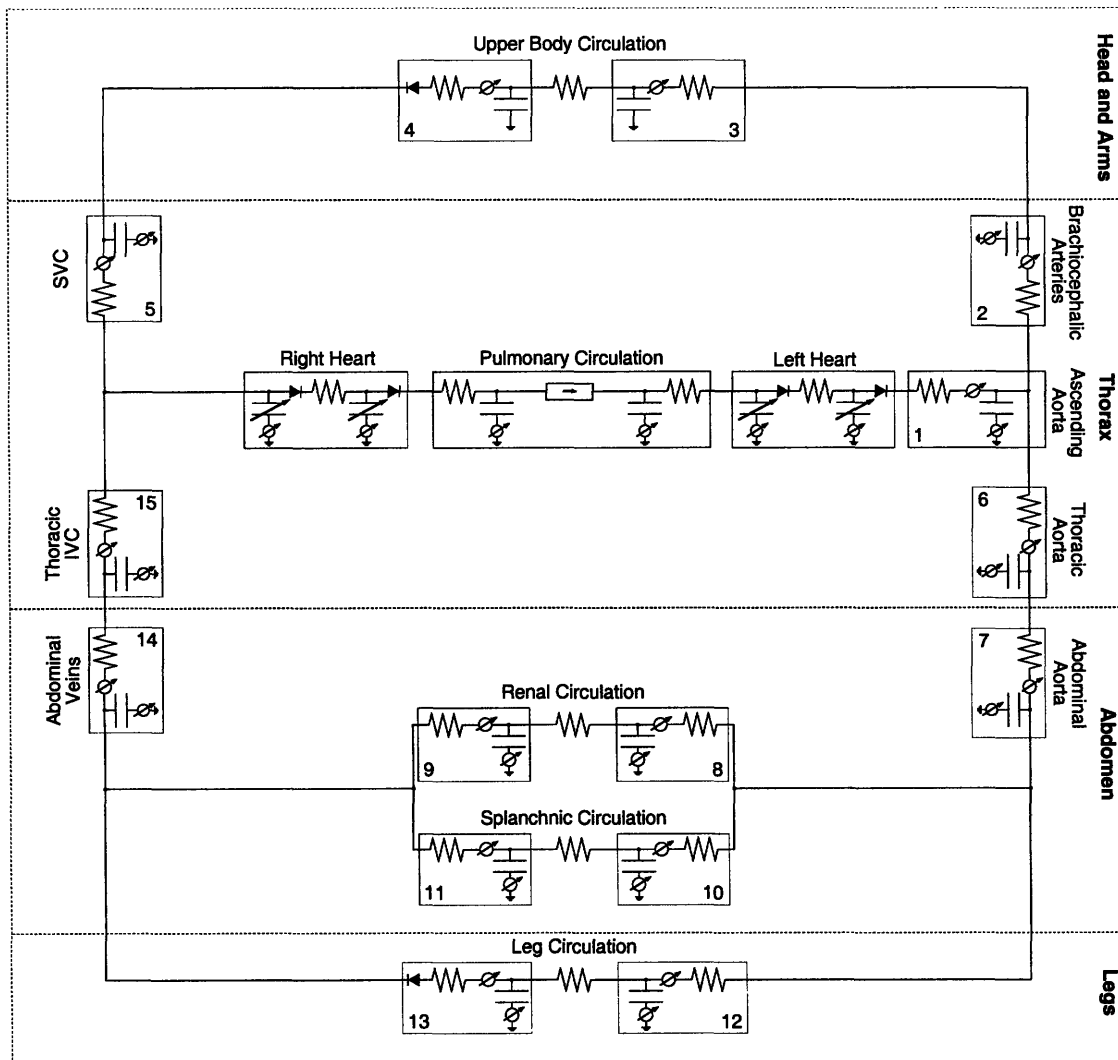


Figure 2.2: Circuit representation of Heldt's model. Figure taken from Heldt [2]

Figure 2.1:

$$\begin{aligned} q_n &= \frac{P_{n-1} - P_n + P_h}{R_n} \\ q_{n+1} &= \frac{P_n - P_{n+1}}{R_{n+1}} \\ q_c &= \frac{d}{dt} V_n = \frac{dV_n}{d(P_n - P_e)} \cdot \frac{d}{dt}(P_n - P_e) = \frac{dV_n}{d\Delta P_n} \cdot \frac{d\Delta P_n}{dt} \end{aligned}$$

where ΔP_n is the transmural pressure of the compartment. Since most of the compartments will be modeled as having linear pressure-volume relationships, $\frac{dV_n}{d\Delta P_n}$ can be simplified to C_n , the compartmental compliance; C_n represents the incremental compartmental compliance in compartments with non-linear pressure-volume relationships. We then combine the above expressions for the flows to arrive at an expression for the change of transmural pressure with respect to time:

$$\frac{d}{dt} \Delta P_n = \frac{P_{n-1} - P_n + P_h}{C_n R_n} - \frac{P_n - P_{n+1}}{C_n R_{n+1}} \quad (2.1)$$

Thus, the equations for the systemic circulation of our model can be derived by using the above expression for the time derivative of the transmural pressure for each compartment and coupling the equations for the various compartments according to the branching in Figure 2.2. Thus, the systemic circulation can be described by 15 coupled first-order differential equations. It should be noted that the total volume in each compartment is the sum of the zero-pressure filling volume (V_0) and the distending volume (V_d), so that $V = V_0 + V_d$. It is the distending volume, V_d , that is directly dependent on the transmural pressure ΔP , whereas the zero-pressure filling volume V_0 remains constant with respect to transmural pressure. It is important to be clear as to which anatomical structures each compartment in Figure 2.2 represents, as this will affect the distribution of volume and flow in each compartment. As Heldt mentions, the upper body compartment represents the circulation of the head, the neck, and the upper extremities. The model assumes that the upper body compartment thereby accounts for 10% of skeletal muscle mass, one third of the skin, and one half of the skeleton. The kidneys and adrenal glands are represented by

Hemodynamic Model

the renal compartment. The splanchnic compartment represents the gastrointestinal tract, one third of the skin, and one half of the adipose tissue. The leg compartment represents the pelvic circulation and the lower extremities. Thus, the model assumes the leg compartments contain the pelvic organs, 90% of skeletal muscle mass, one half of the skeleton, one third of the skin, and one half of the adipose tissue [2].

2.2.1 Non-linearities

As described in the previous section, most of the systemic circulation can be described by a set of differential equations that are linear in their arguments. However, there are certain aspects of the systemic circulation that cannot be accurately modeled by a linear system, and thus non-linearities need to be taken into account. One such aspect is the fact that the systemic circulation contains valves in certain areas of the venous circulation which only allow unidirectional flow. In particular, valves are found in the veins in the anatomical structures modeled by the upper body and leg compartments. As discussed in the introduction to this chapter, valves in the cardiovascular system are modeled by diodes in the electric circuit analog. Thus, diodes are shown in Figure 2.2 immediately following the upper body venous compartment and the venous leg compartment. As shown in the figure, the valves only allow flow in the downstream direction (towards the vena cava).

As discussed in Section 2.2, most of the compartments are modeled as having a linear pressure-volume relationship, and thus are modeled as having a capacitor with constant compliance C_n (with respect to transmural pressure). The vascular volume of a typical blood vessel rises approximately linearly at low transmural pressures, although at high transmural pressures the vessel compliance decreases with increasing transmural pressure and the vessel reaches an elastic limit. As most vessels operate in a range of transmural pressures over which the pressure-volume relationship is essentially linear, it is realistic to model the pressure-volume relationship of such vessels as being linear. However, as will be discussed in Section 2.5, certain orthostatic stress conditions can lead the transmural pressure in vessels, which normally operate in the linear pressure-volume, regime to fall into

2.2 Systemic Circulation

negative regimes of transmural pressure, which will cause collapsing of the vessel. Thus the linear pressure-volume model will no longer hold under such conditions. Furthermore, as Heldt points out, under conditions of normal orthostatic stress, venous transmural pressures can enter regimes in which the pressure-volume relation is non-linear [2, 11, 12]. Therefore, it is necessary to model the non-linear pressure-volume relation in venous compartments, which can be exposed to such levels of transmural pressure. The relation between total volume, V_t , and transmural pressure is modeled (by Heldt [2]) according to

$$V_t = V_0 + \frac{2V_{max}}{\pi} \cdot \arctan\left(\frac{\pi C_0}{2V_{max}} \cdot \Delta P\right) \quad \text{for } \Delta P > 0$$

in the splanchnic venous compartment, leg venous compartment, and abdominal venous compartment. Here, V_{max} is the distending volume limit of the particular compartment, C_0 is the nominal vascular compliance of the compartment at zero transmural pressure, and V_0 is the zero-pressure filling volume of the compartment.

The model of the systemic circulation is now fully described in terms of its parameters. Each compartment in the systemic circulation needs a specification of anatomical vertical length, resistance, zero-pressure filling volume, and compliance (or nominal compliance and maximum distending volume for compartments with non-linear pressure-volume relations). In addition, resistances must be specified for the microcirculation in the upper body, renal, splanchnic, and leg compartments. The parameters are tabulated in Table 2.1 for the systemic arterial circulation, Table 2.2 for the systemic venous circulation, and in Table 2.3 for the systemic microcirculation. All data taken from [2].

	Compartment Index							
	1	2	3	6	7	8	10	12
C $\frac{\text{ml}}{\text{mmHg}}$	0.28	0.13	0.42	0.21	0.10	0.21	0.42	0.42
V_0 ml	21	5	200	16	10	20	300	200
R PRU	0.007	0.003	0.014	0.011	0.010	0.010	0.07	0.09
h cm	10.0	4.5	20.0	16.0	14.5	0.0	10.0	106

Table 2.1: Parameter values for the systemic arterial compartments. Compartment indices from Figure 2.2

Hemodynamic Model

		Compartment Index						
		4	5	9	11	13	14	15
C	ml/mmHg	7	1.3	5	50	27	1.3	0.5
V_0	ml	645	16	30	1146	716	79	33
R	PRU	0.11	0.028	0.11	0.07	0.10	0.019	0.008
h	cm	20.0	14.5	0.0	10.0	106	14.5	6.0

Table 2.2: Parameter values for the systemic venous compartments. Compartment indices from Figure 2.2

		Microcirculation			
		upper body	kidneys	splanchnic	legs
R	PRU	4.9	5.2	3.3	4.5

Table 2.3: Parameter values for the systemic microvascular resistances.

2.3 Cardiopulmonary Circulation

As described in Section 1.2.1, the cardiopulmonary circulation consists of the heart and lungs. The heart is divided into a left heart and right heart, each having its own atrium and ventricle. The right heart receives blood from the systemic veins and pumps blood into the pulmonary arteries. The blood flows through the pulmonary circulation and from the pulmonary veins into the left heart, which pumps the blood back into the systemic arteries. The model of the cardiopulmonary circulation follows from circuit diagram in Figure 2.2. Our model of the cardiac compartments will follow Heldt's model without modification, however, we will simplify the model of the pulmonary circulation.

2.3.1 Cardiac Compartments

The model for the cardiac circulation models the four cardiac chambers as four cardiac compartments: the right atrium, the right ventricle, the left atrium, and the left ventricle. Each cardiac compartment is modeled in a similar way to a vascular vessel, except for two very significant differences. First, unlike the elastance of a vascular compartment, the elastance of a cardiac compartment is not constant with respect to time. Second, there are valves allowing only unidirectional flow at the inlet and outlet of both the right and left

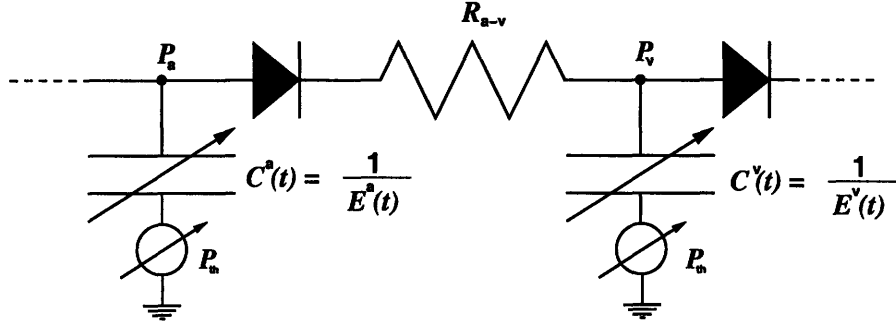


Figure 2.3: Circuit representation of atrial and ventricular cardiac compartments. P_a and P_v : atrial and ventricular luminal pressures; P_{th} : intrathoracic pressure; $C^a(t)$ and $C^v(t)$: atrial and ventricular compliances; $E^a(t)$ and $E^v(t)$: atrial and ventricular elastances. R_{a-v} : atrio-ventricular flow resistance. Figure taken from Heldt [2]

	Right Heart		Left Heart	
	Atrium	Ventricle	Atrium	Ventricle
E_{es} $\frac{\text{mmHg}}{\text{ml}}$	0.74	1.3	0.61	2.5
E_d $\frac{\text{mmHg}}{\text{ml}}$	0.30	0.07	0.50	0.13
V_0 ml	14	46	24	55
R_{a-v} PRU		0.005		0.010

Table 2.4: Cardiac Model Parameters. Values taken from [2]

ventricles. This is represented in Figure 2.3.

Data of the time-varying elastance for human left ventricles [13] justifies a functional representation thereof described by Equation 2.2 (from [2]) with the assumption that the time for early diastolic relaxation, T_d^r is one half of the systolic time interval T_s .

$$E(t) = \begin{cases} E_d + \frac{E_{es}-E_d}{2} \cdot \left\{ 1 - \cos \pi \cdot \frac{t}{T_s} \right\} & 0 \leq t \leq T_s \\ E_d + \frac{E_{es}-E_d}{2} \cdot \left\{ 1 + \cos 2\pi \cdot \frac{t-T_s}{T_s} \right\} & T_s < t \leq \frac{3}{2}T_s \\ E_d & \frac{3}{2}T_s < t \end{cases} \quad (2.2)$$

Here $E(t)$ is the time-varying cardiac elastance, E_d is the end-diastolic elastance, and E_{es} is the end-systolic elastance. The shape of the normalized time-varying elastance waveform is assumed to be the same for all four cardiac chambers, whereas the parameters will vary from chamber to chamber. The parameters for the cardiac compartments are tabulated in Table 2.4.

Hemodynamic Model

	T_s^a	T_s^v	T_{a-v}
time s	$0.25\sqrt{T_{RR}}$	$0.37\sqrt{T_{RR}}$	$0.19\sqrt{T_{RR}}$

Table 2.5: Values for cardiac timing parameters. Values taken from [2].

As the time-varying cardiac elastance function $E(t)$ depends on the systolic time interval T_s , it is also necessary to detail an expression for it. The systolic time interval differs in the atria (T_s^a) and the ventricles (T_s^v); furthermore, there is a delay T_{a-v} between the onsets of atrial and ventricular contraction. These three parameters are directly proportional to $\sqrt{T_{RR}}$, where T_{RR} denotes the R-R interval length (or the inter-beat interval) [2]. As will be discussed in Section 2.3.3, the inter-beat interval of the current heartbeat cannot be known until the onset of the next heartbeat; therefore, these cardiac timing parameters will depend on the inter-beat interval from the previous heartbeat. These dependencies are listed in Table 2.5.

2.3.2 Pulmonary Circulation

As shown in Figure 2.2, the pulmonary circulation is modeled as having one arterial compartment and one venous compartment connected by the pulmonary microcirculation. Heldt models in detail the effect of changes in luminal and extra-luminal pulmonary pressure on the flow through the pulmonary microvasculature; however, such a detailed model is not necessary for our purposes, as the difference in the response of the cardiovascular system to orthostatic stress would be negligible. Therefore, we simplify the model of the pulmonary microcirculation to a single resistor with resistance R_p , just as was the case in the microcirculation of a systemic vascular compartment. Thus the pulmonary circulation is modeled as 2 vascular compartments connected in series by a resistor. The parameters for the pulmonary circulation are tabulated in Table 2.6.

2.3.3 Cardiac Pacemaker

The model of the heart described in Section 2.3.1 depends upon the R-R interval length T_{RR} , which takes a nominal value, I_0 , of 895 ms. According to Heldt, however, the true R-R interval upon which the cardiac timing parameters depend is computed as the time-interval between the onset of subsequent heartbeats. The contraction of the heart muscle is initiated by cardiac excitation, which occurs upon the spontaneous depolarization of cardiac pacemaker cells in the sinoatrial node; this phenomenon is known as the automaticity of cardiac pacemaker cells. When the transmembrane potential of these cells rises above a specific threshold potential, the cell membrane rapidly reverses polarity generating an action potential. The model of the cardiac pacemaker generates the onset times of cardiac excitation which corresponds to the threshold-crossing of the transmembrane potential. Our model implements an Integral Pulse Frequency Modulation (IPFM) model to represent the dynamics of the transmembrane potential during diastole [2, 14, 36]. The model represents the transmembrane potential as a function $M(t)$ whose value depends on the history of automaticity and neural (control) input (the latter is discussed in Chapter 3) since the onset of the last cardiac excitation time:

$$M(t) = \int_{t_{k-1}}^t m(t)dt = \int_{t_{k-1}}^t (m_0 + m_r(t))dt$$

where t_{k-1} represents the time of the onset of the last cardiac excitation, m_0 represents the automaticity, and $m_r(t)$ is the control input from the arterial baroreflex system, to be discussed in Chapter 3. The k th beat starts at time t_k when $M(t)$ reaches a threshold Γ and the refractory period of the cardiac pacemaker cell has passed. The refractory period

	Pulmonary Compartments	
	Arteries	Veins
C	ml/mmHg	3.4 9.0
V_0	ml	160 430
R	PRU	0.006 0.006
R_p	PRU	0.07

Table 2.6: Parameter values for pulmonary compartments. Values taken from [2].

is defined as the time immediately after the onset cardiac excitation during which another action potential cannot occur. It is set to be $0.2 \cdot (t_{k-1} - t_{k-2})$. So the condition for a new beat to occur is then:

$$\int_{t_{k-1}}^{t_k} m(t) dt = M(t_k) \geq \Gamma \quad \text{and} \quad t_k - t_{k-1} \geq 0.2 \cdot (t_{k-1} - t_{k-2}).$$

Based on the implementation of neural feedback in the model, a natural choice for $m(t)$ is the inverse of the instantaneous R-R interval $I(t)$, so that:

$$m(t) = \frac{1}{I(t)} = \frac{1}{I_0 + \Delta I_{AB}(t)}$$

where I_0 is the nominal R-R interval and $\Delta I_{AB}(t)$ represents the control input to the change in the instantaneous R-R interval from the arterial baroreflex system. Here the value for the threshold Γ is set to 1.0, so that, in the absence of any control input, the R-R interval simplifies to I_0 , the nominal R-R interval.

2.4 Modeling Orthostatic Stress

The type of orthostatic stress we are primarily interested in modeling is centrifugation, and we develop a novel framework for modeling the effects of centrifugation stress on the cardiovascular system. For purposes of completeness, we will also present the models for the orthostatic stress resulting from an upright-tilt of the body from a supine to upright position and from lower-body negative pressure (both modeled by Heldt [2]). As discussed in the introduction to this chapter, the effects of orthostatic stress which results in a vertical pressure gradient on a compartment is modeled by a pressure source in series with the compartment. This is how both upright-tilt and centrifugation will be modeled. The value of the pressure source will depend on the vertically downwards acceleration which results from the orthostatic stress. We will follow Heldt's model for upright tilt and LBNP simulations and will propose a new model for centrifugation simulations.

2.4.1 Upright Tilt

In the constant accelerational field of gravity, the hydrostatic pressure gradient imposed on a tube by tilting it upwards is known to be

$$P_h = \rho g h \sin \alpha \quad (2.3)$$

where ρ is the density of the fluid, g is gravitational acceleration, h is the length of the tube, and $\alpha(t)$ is the tilt angle of the tube (from the ground). In modeling the hydrostatic pressure gradients in a vascular compartment, ρ is the density of blood, and h is the effective height of the vascular compartment. Note that h is termed the effective height of the compartment in contrast to the anatomical height of the compartment. Tables 2.1 and 2.2 list the the anatomical heights of the various compartments in the systemic circulation. As each compartment is a lumped representation of various anatomical structures, the effective height h of the compartment is then assumed to be one half of the anatomical vertical heights; the exception to this is in the legs, where the effective height is one third of the anatomical height. This effective height is employed in order to properly simulate the representative variables of the compartment. In other words, the effective height can be viewed as a compliance-weighted height, so that the stress simulation can properly account for the volume distribution of the compartment. The time course of the tilt-angle $\alpha(t)$ follows a raised cosine model according to:

$$\alpha(t) = \begin{cases} 0 & \text{for } t < t_0 \\ \alpha_{\max} \cdot \frac{1}{2} \cdot (1 - \cos(\pi \frac{t-t_0}{\Delta t})) & \text{for } t_0 \leq t \leq t_0 + \Delta t \\ \alpha_{\max} & \text{for } t > t_0 + \Delta t \end{cases} \quad (2.4)$$

where α_{\max} is the maximum tilt angle in the upright tilt simulation, t_0 is the onset time of upright tilt, and Δt is the time to reach α_{\max} from the onset time.

Changes in intra-thoracic pressure Studies by Mead and Gaensler [16] and Ferris et al. [17] showed that the intra-thoracic pressure P_{th} dropped over a similar time course in

Hemodynamic Model

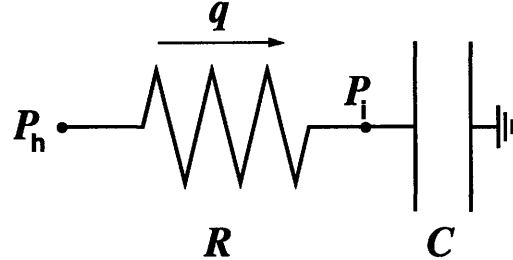


Figure 2.4: RC model of interstitial compartment. Figure taken from Heldt [2]

response to gravitational stress. This drop in intrathoracic pressure occurs as a result of the weight of the liver pulling down on the thoracic compartment. The time course of P_{th} is modeled as depending on the tilt angle $\alpha(t)$, according to:

$$P_{th}(t) = P_{th0} - 3.5 \sin \alpha_{max} \sin \alpha(t) \quad (2.5)$$

where P_{th0} is the nominal intrathoracic pressure.

Volume loss to interstitium Furthermore, changes in hydrostatic pressure components as a result of orthostatic stress affect the transcapillary pressure gradients that govern transcapillary fluid exchange resulting in an overall increase in transcapillary fluid flow and decrease in intravascular volume. Based on studies on the nature of the transcapillary fluid flow during orthostatic stress [18–27], the proposed model for simulating transcapillary fluid flow is an additional interstitial compartment, modeled as a single RC component, for each systemic compartment that loses intravascular volume to transcapillary flow, as shown in Figure 2.4. However, as Heldt points out [2], such an approach would add two parameters per compartment, as well as additional state variables, and unnecessarily increase computational complexity. To save on computational cost, the transcapillary flow can be solved analytically beforehand and simply be subtracted from the venous return at the designated compartments. The solutions depend on two parameters: the time constant $\tau = RC$ and the maximal volume lost from the intravascular volume $V_{max} = P_h C$. Heldt lists the analytical solutions to the transcapillary flow and volume which are reproduced in Appendix A.

For upright tilt simulations, $\tau = R \cdot C = 4.6$ min and $V_{max} = 700$ ml to a tilt to 85° . The compartments from which the interstitial fluid flow is subtracted are the splanchnic venous, leg venous, and abdominal venous compartments. The fraction of leakage current and volume loss assigned to each of these compartments is given by the proportion of each compartment's maximum hydrostatic pressure to the combined maximum hydrostatic pressure of the three compartments, so for compartment n , we have:

$$\begin{aligned} V^n(t) &= \frac{P_{h,max}^n}{\sum_i P_{h,max}^i} \cdot V(t) \\ q^n(t) &= \frac{P_{h,max}^n}{\sum_i P_{h,max}^i} \cdot q(t) \end{aligned}$$

2.4.2 Lower Body Negative Pressure

As discussed in Section 1.1, a lower-body negative pressure intervention involves rapidly reducing the external pressure around the lower extremities of the body causing the blood to pool in this region. Therefore, LBNP experiments are modeled by dropping the external pressure in the leg compartments. As in the upright tilt simulation, the time course of the change in external pressure is described by an (inverted) raised cosine model according to:

$$P_{ext}(t) = \begin{cases} 0 & \text{for } t < t_0 \\ P_{max} \cdot \frac{1}{2} \cdot (1 - \cos(\pi \frac{t-t_0}{\Delta t})) & \text{for } t_0 \leq t \leq t_0 + \Delta t \\ P_{max} & \text{for } t > t_0 + \Delta t \end{cases} \quad (2.6)$$

where P_{max} is the maximal external negative pressure applied during the LBNP experiment, t_0 is the onset time of LBNP, and Δt is the time duration to reach P_{max} after the onset of LBNP. Based on studies on the changes in plasma volume during LBNP interventions [28, 29], interstitial fluid flow during LBNP is modeled in the same method as with upright tilt with the time constant of the model τ remaining the same and the maximal plasma volume loss following

$$V_{max} = 491 \text{ ml} \cdot \frac{P_{max}}{70 \text{ mmHg}}.$$

2.4.3 Centrifugation

Our model for centrifugation will use the hydrostatic pressure sources P_h to account for the hydrostatic pressure gradient resulting from centrifugation. As discussed in Section 1.1, the nature of centrifugal stress is markedly different from that of gravitational stress, as the radial acceleration resulting from centrifugation is a direct function of the distance from the center of rotation. In this context, it becomes convenient to view the human body in terms of cylindrical coordinates, with the center of the coordinate system lying at the center of rotation of the centrifuge. The body is then lying on the centrifuge with the feet pointing in the radially outward direction. The hydrostatic pressure gradient through a differentially thick radial cross-section is given by

$$dP_h = \rho a(r) dr$$

where $a(r)$, the radially dependent centrifugal acceleration, is given by

$$a(r) = \omega^2(t)r$$

and where $\omega(t)$ is the angular velocity of the centrifuge at time t .

Combining the above expressions and integrating over the effective height of the compartment, we have

$$\begin{aligned} P_h &= \int_{R_i}^{R_o} \rho \omega^2(t) r dr \\ P_h &= \frac{1}{2} \rho \omega^2(t) (R_o^2 - R_i^2) \end{aligned} \tag{2.7}$$

where the inlet radius R_i is the distance of the superior end of the compartment from the center of rotation and the outlet radius R_o is the sum of the effective height of the compartment and the inlet radius ($R_o = R_i + h$). As before, the effective height h of the compartment is one half of its anatomical height, again, with an exception to the legs, where the effective height is one third of the anatomical height. In order to compute the different values of R_i for each compartment of the systemic circulation, we can simply sum

2.4 Modeling Orthostatic Stress

		Compartment Index														
		1	2	3	4	5	6	7	8	9	10	11	12	13	14	15
$R_i - d$	cm	24.5	20.0	0	0	20	24.5	40.5	55.0	55.0	55.0	55.0	55.0	40.5	34.5	

Table 2.7: Values for $R_i - d$. Compartment indices from Figure 2.2

the distance of the top of the head from the center of rotation and the anatomical heights of all the sequentially interconnected compartments superior to the compartment under consideration, so that:

$$R_{in} = d + \sum_{j \in S_n} h_{anatomical,j}$$

where S_n contains the indices of compartments that are superior and sequentially interconnected to compartment n , d is the distance of the top of the head from the center of rotation, and $h_{anatomical,j}$ is the anatomical height of compartment j . For convenience, we tabulate the values of $R_i - d$ for each compartment in the systemic circulation in Table 2.7.

The change in intra-thoracic pressure during centrifugation is modeled in a similar way to the upright tilt model. Recalling Equation 2.5, we have for the upright tilt model:

$$P_{th}(t) = P_{th_0} - 3.5 \sin \alpha_{\max} \sin \alpha(t)$$

We must appropriately replace the dependence of this expression on the tilt angle $\alpha(t)$ in order to model the case of centrifugation. In upright tilt, a tilt angle of α corresponds to an acceleration in the head-to-foot direction of $a(t) = g \cdot \sin(\alpha(t))$. Therefore, we can rearrange this relation to get

$$\sin(\alpha(t)) = \frac{a(t)}{g} \quad \text{and} \quad \sin(\alpha_{\max}) = \frac{a_{\max}}{g}$$

where a_{\max} is the maximum acceleration.

Thus, the change in intra-thoracic pressure during centrifugation is modeled as

$$P_{th}(t) = P_{th_0} - 3.5 \cdot \frac{a_{\max} \cdot a(t)}{g^2}$$

Hemodynamic Model

$$P_{th}(t) = P_{th_0} - 3.5 \cdot \frac{(r + d)^2 \cdot \omega_{\max}^2}{g^2} \cdot \omega^2(t) \quad (2.8)$$

where $a(t)$ and a_{\max} are taken at upper portion of the abdomen ($r = 55$ cm), as the change in intra-thoracic pressure results from the weight of the liver (which is located in the right upper abdomen) on the thoracic compartment.

Furthermore, our model of interstitial fluid flow during centrifugation will also follow the same form of the model for interstitial fluid flow during upright tilt. Again, the time constant τ is kept the same as in the upright tilt model. The expression for V_{\max} in the model for upright tilt given in Section 2.4.1 is

$$V_{\max} = 700 \text{ ml} \cdot \frac{\sin \alpha_{\max}}{\sin 85^\circ}.$$

Again, making the substitution $\sin \alpha_{\max} = \frac{a_{\max}}{g}$, we have

$$V_{\max} = 700 \text{ ml} \cdot \frac{a_{\max}}{g \cdot \sin 85^\circ}$$

$$V_{\max} = 700 \text{ ml} \cdot \frac{(r + d) \cdot \omega_{\max}^2}{g \cdot \sin 85^\circ}.$$

Again, a_{\max} , the maximum centrifugal acceleration, is taken at the upper abdomen ($r = 55$ cm). As with the upright tilt model, the interstitial fluid flow is subtracted from the splanchnic venous, leg venous, and abdominal venous compartments, and the fraction of leakage current and volume loss assigned to each of these compartments is given by the proportion of the maximal hydrostatic pressure of the compartment under consideration to the combined maximal hydrostatic pressures of the three compartments.

2.5 Modeling Vessel Collapse

As alluded to in Section 2.2.1, certain levels of orthostatic stress can lead to the transmural pressure in a compartment becoming negative. Under such conditions, the volume in the

vessels represented by a compartment gradually decreases until it is fully drained. As a vessel is being drained of its volume, it admits less fluid flow, until it is fully collapsed and exhibits zero admittance to flow. As such, modeling the compartments that exhibit vessel collapse as a linear single resistor-capacitor network fails to capture this phenomenon. Indeed, the linear model poses the risk of actually simulating an injection of volume into the cardiovascular system, if the (negative) distending volume (i.e. the volume being drained from the compartment) increases the zero-pressure filling volume V_0 of the compartment. Furthermore, the linear resistor model impedes fluid flow at a resistance that is independent of the volume in the vessel. The following sections will discuss how we will modify Heldt's model to account for this phenomenon.

2.5.1 Pressure-Volume Relationship

Although, under normal conditions, most blood vessels in the systemic circulation operate in a range of transmural pressures where the pressure-volume relationship is approximately linear, the entire pressure-volume relationship of a blood vessel is non-linear. As discussed in Section 2.2.1, the pressure-volume relationship is approximately linear over low (positive) transmural pressures and reaches an elastic limit as the transmural pressure increases beyond a certain range. By definition, when the transmural pressure is zero, the volume of a vessel is equal to its zero-pressure filling volume, V_0 . As the transmural pressure decreases below zero into negative ranges, the volume decreases approximately linearly (more accurately, exponentially) from V_0 with a significantly smaller compliance (which we will call C_{neg}) until it reaches zero and the vessel is fully collapsed. We will call the transmural pressure where the vessel first reaches zero volume ΔP_0 , the zero-volume pressure. As the transmural pressure decreases below ΔP_0 , the vessel remains fully collapsed and the volume remains at zero. This is illustrated in Figure 2.5 where data published by Ryder et al. shows the pressure-volume relationship of a common iliac vein [30]. From Figure 2.5, we see that the zero-volume pressure ΔP_0 for the iliac vein is approximately -5 mmHg; we will use this value for ΔP_0 in all compartments that exhibit vessel collapse.

Hemodynamic Model

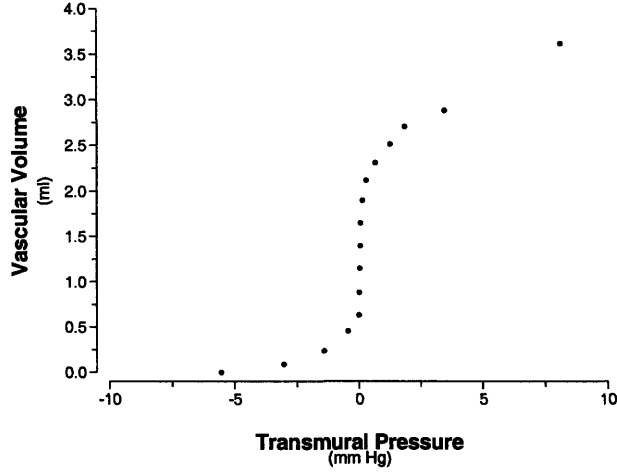


Figure 2.5: Pressure-volume relation of a common iliac vein. Figure from [2]. Data adapted from [30]

We will model the volume of the compartments exhibiting vessel collapse as a piecewise linear function of the transmural pressure in the range of negative transmural pressures. In the range of non-negative transmural pressures, the pressure-volume relationship will remain as discussed in Sections 2.2 and 2.2.1. Denoting the model for volume as a function of transmural pressure prior to our discussion of vessel collapse as $V_+(\Delta P)$ (in order to account for the non-linear pressure-volume relationships discussed in earlier sections), we can describe our model of the pressure-volume relationship in compartments exhibiting vessel collapse as

$$V(\Delta P) = \begin{cases} 0 & \text{for } \Delta P < \Delta P_0 \\ \frac{V_0}{\Delta P_0} \cdot \Delta P + V_0 & \text{for } \Delta P_0 \leq \Delta P < 0 \\ V_+(\Delta P) & \text{for } \Delta P \geq 0 \end{cases} \quad (2.9)$$

It is clear from the above that the draining compliance C_{neg} is given by $C_{neg} = \frac{V_0}{\Delta P_0}$. Equation 2.9 is plotted in Figure 2.6.

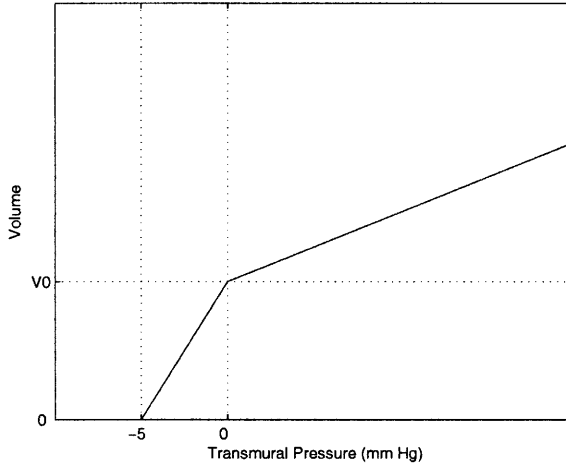


Figure 2.6: Model for the Pressure-Volume Relation for a Collapsible Vessel.

2.5.2 The Starling Resistor

Having specified our model for the pressure-volume relationship of a compartment exhibiting vessel collapse, we move on to detail the model for fluid flow in such compartments. A well-established model for fluid flow through collapsible tubes is known as the Starling resistor [31]. An idealized Starling resistor operates in two states: (1) completely collapsed, where no flow is allowed and there is infinite flow resistance, or (2) conducting with flow resistance R_0 . The steady-state behavior of the Starling resistor can then be described by its flow in terms of the three pressure differences ($P_{in} - P_e$, $P_{out} - P_e$, and $P_{in} - P_{out}$) [32] by:

$$q(P_{in}, P_{out}, P_e) = \begin{cases} 0 & \text{if } P_{in} - P_e < 0 \text{ and } P_{out} - P_e < 0 \quad (\text{Zone I}) \\ \frac{P_{in} - P_e}{R_0} & \text{if } P_{in} - P_e > 0 \text{ and } P_{out} - P_e < 0 \quad (\text{Zone II}) \\ \frac{P_{in} - P_{out}}{R_0} & \text{if } P_{in} - P_e > 0 \text{ and } P_{out} - P_e > 0 \quad (\text{Zone III}) \end{cases} .$$

In Zone I, the external pressure is greater than both the inlet and outlet pressures, so the tube is fully collapsed and no flow is allowed. In Zone III, both the inlet and outlet pressures exceed the external pressure, so the tube is not collapsed and behaves as a linear

resistor. In Zone II, when the external pressure exceeds the outlet, but not the inlet pressure, the tube continuously switches between the collapsed and conducting states and detailed analyses of the structural mechanics of the tube [33–35] reveal that the flow is governed by the difference between the inlet and external pressures and is not influenced by the outlet pressure.

While this model is perfectly plausible for modeling the flow through collapsible vessels in the cardiovascular system, its implementation into our model of the cardiovascular system is problematic. The steady-state Starling resistor model, while detailing the flow through a collapsible vessel, does not account for the volume of a vessel. This poses a problem for us as we need to implement a model for the flow through a collapsible vessel along with a model of its pressure-volume relationship as detailed in Section 2.5.1; implementing the steady-state Starling resistor in our model would then decouple these two inherently coupled vessel characteristics. These problems become apparent in simulating our model with the flow defined by the steady-state Starling resistor: the volumes of compartments modeled as collapsible compartments still fall into the unrealistic negative range. Therefore, having discussed why modeling the flow through a collapsible compartment by the well-established steady-state Starling resistor model will not work for our purposes, we are in need of a model for the flow which inherently accounts for the volume of the compartment.

2.5.3 Volume-Dependent Resistance

An initial idea for modeling the flow through a collapsible compartment was to model the flow according to the behavior of the instantaneous idealized Starling resistor (as opposed to the steady-state Starling resistor described in the previous section), which can be modeled as a function of the vessel volume. Again, an idealized Starling resistor takes one of two states: (1) collapsed where the resistance to flow is infinite and no flow is admitted and (2) conducting with nominal resistance R_0 . Thus, the volume-dependent resistance $R(V(t))$ in

a compartment exhibiting vessel collapse is given by

$$R(V(t)) = \begin{cases} \infty & V = 0 \\ R_0 & V > 0 \end{cases}$$

Such a model for the resistance, however, also poses a problem in implementation due to the discrete switching dynamics. In simulating such a model, once the volume reaches zero, the flow out of the vessel switches to zero, which almost immediately causes the volume to increase by a differential amount, which then causes the flow to switch back to conducting. The simulator switches the resistance between the two values over infinitesimally small time steps attempting to detect the precise time when zero-crossing occurs; the result is a chattering effect in the pressure and an inability of the numerical solver to move forward in time. In order to avoid this problem, a similar model can be implemented where the resistance rises exponentially from its nominal value at the unstressed volume V_0 to an extremely large value at zero volume (which would pose a practically infinite resistance, allowing an infinitesimally small flow). Furthermore, under the high levels of orthostatic stress where vessel collapse may occur, it is perfectly conceivable that flow through a compartment may also reverse direction, therefore the model will also account for the direction of the flow so that the volume-dependent resistor is on the direction of the outflow of the compartment. Thus, following the notation in Figure 2.1, our model for the volume-dependent resistors on each side of compartment n is written as:

$$R_n(V_n(t)) = \begin{cases} R_{0n} + R_{\text{high}} \cdot e^{\ln(\epsilon/R_{\text{high}}) \cdot \frac{V_n(t)}{V_{0n}}} & P_{n-1} < P_n \\ R_n(V_{n-1}(t)) & P_{n-1} \geq P_n \end{cases} \quad (2.10)$$

$$R_{n+1}(V_n(t)) = \begin{cases} R_{0n+1} + R_{\text{high}} \cdot e^{\ln(\epsilon/R_{\text{high}}) \cdot \frac{V_n(t)}{V_{0n}}} & P_{n+1} < P_n \\ R_{n+1}(V_{n+1}(t)) & P_{n+1} \geq P_n \end{cases} \quad (2.11)$$

where compartments n , $n+1$, and $n-1$ (the current compartment, the compartment downstream of n , and the compartment upstream of n , respectively) are all assumed to exhibit vessel collapse (hence the terms $R_{n+1}(V_{n+1}(t))$ and $R_{n+1}(V_n(t))$), R_{0n} is the nominal resis-

Hemodynamic Model

tance of R_n , R_{high} is an extremely high resistance value that simulates infinite resistance, and ϵ is an extremely small number that is added to the nominal resistance when the compartment volume is at V_0 , the unstressed volume. Equation 2.11 is plotted in Figure 2.7 assuming blood is flowing in the downstream direction.

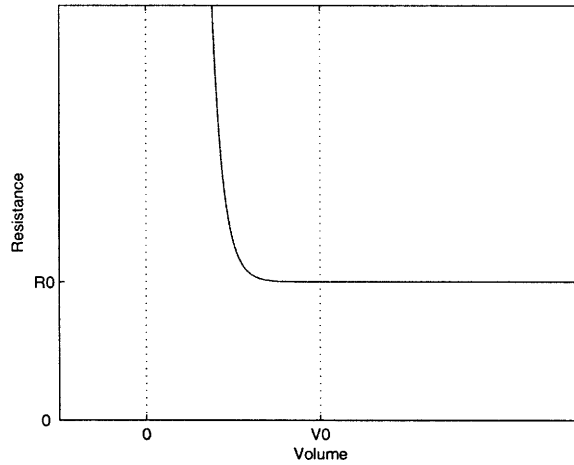


Figure 2.7: Model for Volume-Dependent Resistance for a Collapsible Vessel.

This model for the volume dependent resistance of a compartment exhibiting vessel collapse inherently couples the fluid flow through the compartment with the volume of the compartment. Combining Equations 2.9, 2.10, and 2.11, we have developed a complete model for vessel collapse. As the compartmental volume and flow are now coupled, simulations at even extreme levels of orthostatic stress show that compartmental volume does not become negative in compartments modeled as exhibiting vessel collapse. Furthermore, as the model is essentially a continuous volume-dependent version of the well-established (instantaneous) idealized Starling resistor, we expect it to be physiological.

In order to decide which compartments to model with the feature of collapsibility, we simulate the open-loop hemodynamic model without modeling collapsibility into any compartment at an extremely high level of orthostatic stress (centrifugation at 100 $\frac{\text{rev}}{\text{min}}$) and find which compartments have a volume less than the compartmental unstressed volume (and are thus draining) during orthostatic stress; these compartments are then modeled with

the feature of collapsibility. The simulation results show that the following compartments (followed by their compartment indices from Figure 2.2) have volumes falling below the compartmental zero-pressure filling volume during orthostatic stress and are thus modeled with the collapsibility feature: the upper body arteries (3), the upper body veins (4), the superior vena cava (5), the renal veins (9), the splanchnic veins (11), and the abdominal veins (14). Furthermore, we set the values of R_{high} and ϵ to $R_{high} = 1000$ PRU and $\epsilon = 10^{-5}$ PRU.

2.6 Model Implementation

2.6.1 Platform

We developed the model primarily in Simulink and used a previous six-compartment model developed in Simulink by Samar [10] as the skeleton for our code, augmenting it by adding compartments, parameters, a framework for orthostatic stress simulations, and the various other features described in previous sections of this chapter. Simulink, which is tightly integrated with MATLAB, is a particularly useful tool for modeling system dynamics as it provides many predefined functions, numerical integration techniques, and analytical tools. The MATLAB m-file environment was also used to determine initial conditions and for post-simulation data processing steps.

2.6.2 Choice of State Variables

The entire open-loop hemodynamic model described in this chapter is given by a system of 21 first-order non-linear time-varying differential equations. The model as described by Heldt [2] gives the differential equations for \dot{P}_n , the time derivative of the luminal pressures for each compartment, which suggests a choice of the compartmental luminal pressures as state variables for the model. This choice is intuitive and poses no problems. However, we must take into consideration the repercussions of the choice of state variables on the

Hemodynamic Model

numerical solution to the system of equations. Recalling Equation 2.1, the time derivative of the luminal pressure in a compartment is given as

$$\frac{d}{dt}P_n = \frac{P_{n-1} - P_n + P_h}{C_n R_n} - \frac{P_n - P_{n+1}}{C_n R_{n+1}} + \frac{d}{dt}P_e \quad (2.12)$$

again, where C_n is the incremental compliance $\frac{dV}{d(P_n - P_e)}$. Changes in P_e during orthostatic stress simulations causes numerical integration errors when numerically computing the value of $\frac{d}{dt}P_e$. Rewriting Equation 2.12 with the transmural pressure ΔP as the state variable, we have:

$$\frac{d}{dt}\Delta P_n = \frac{(\Delta P_{n-1} + P_e) - (\Delta P_n + P_e) + P_h}{C_n R_n} - \frac{(\Delta P_n + P_e) - (\Delta P_{n+1} + P_e)}{C_n R_{n+1}} \quad (2.13)$$

which suggests using the transmural pressures ΔP_n in each compartment as the state variables. According to Equation 2.13, this choice of a state variable should not pose any numerical errors, as there are no time derivatives to compute. However, the above equation only holds for vascular compartments (which have time invariant pressure-volume relationships); in cardiac compartments, the time-varying nature of the compliance must also be taken into consideration. The differential equation for a cardiac compartment, following the discussion in Section 2.3.1, is:

$$\begin{aligned} \frac{d}{dt}\Delta P &= \frac{d}{dt}\frac{V_d}{C(t)} \\ &= \frac{1}{C(t)} \cdot \frac{dV_d}{dt} + V_d \cdot \frac{d}{dt}\frac{1}{C(t)} \\ &= \frac{1}{C(t)} \cdot (q_{in} - q_{out}) - (C(t) \cdot \Delta P) \frac{1}{C^2(t)} \cdot \frac{dC(t)}{dt} \\ &= \frac{q_{in} - q_{out} - \Delta P \cdot \frac{dC(t)}{dt}}{C(t)} \end{aligned}$$

Again, there is a numerical computation of a derivative $\frac{dC(t)}{dt}$, which will introduce numerical integration errors as $C(t)$ varies with respect to time (following the inverse of the time-varying elastance function described in Section 2.3.1).

A similar numerical problem involving the compliance is observed in collapsible vas-

cular compartments. Although the compliance in such compartments is constant with respect to time, the identity $C_n = \frac{dV_n}{d\Delta P_n}$ must be computed. However, since the volume V_n in collapsible vessels is modeled as a piecewise linear function of the transmural pressure ΔP , the first derivative of the volume with respect to transmural pressure, $C_n = \frac{dV_n}{d\Delta P_n}$, has discontinuities at the points of compliance change (specifically at $\Delta P = 0$ and at $\Delta P = P_0$). Thus, the numerical computation of incremental compliance in collapsible compartments will introduce numerical integration errors as the transmural pressure crosses the points of discontinuity.

In order, to avoid having to integrate $\frac{dC(t)}{dt}$ in cardiac compartments and $\frac{dV(\Delta P)}{d\Delta P}$ in collapsible vascular compartments, we can follow the strategy employed by Samar [10], and change the state variables in all compartments to the compartmental distending volume $V_d(t)$, so that the state equations for all compartments in our model of the cardiovascular system become very simply:

$$\frac{d}{dt} V_{dn}(t) = q_{inn} - q_{outn}$$

with q_{inn} and q_{outn} having the dependencies on the compartmental pressures described earlier in the chapter. Therefore, in order to avoid numerical errors, we use the distending volumes V_n as the state variables in our model.

2.6.3 Integration Routine

In choosing an integration routine, we note that our model of volume dependent resistance in collapsible compartments introduces a degree of stiffness to the system; by this we mean that our model for volume-dependent resistance can lead to rapid variation in the solution, and thus a numerical solver can become numerically unstable if the simulation step size is not made sufficiently small near points of rapid variation. In order to ensure the that the numerical solver remains numerically stable, we will employ a variable-step solver. Simulink comes with several variable-step solvers built in; our aim is to choose the solver that is the fastest while also being numerically stable. Cycling through the different solvers, we find that the `ode23t` solver best suits our needs. The `ode23t` solver implements the trapezoidal

Hemodynamic Model

rule and is recommended for systems with moderate stiffness. Our model is simulated using the `ode23t` solver setting the maximum step size to 0.01 s and the minimum step size as automatic.

2.6.4 Initial Conditions

In order to obtain the initial conditions for the state variables, we implement a modified version of the method used by Davis to solve for the initial conditions of his six-compartment model [1]. By equating the right ventricular stroke volume and left ventricular stroke volume, and deriving equations for the average blood passing through the remaining compartments under the assumption that the capacitors are not conducting, we form a system of 22 linear algebraic equations (in the luminal pressures and end-systolic and end-diastolic left and right ventricular pressures). A 23rd non-linear equation is obtained on the basis of conservation of volume, setting the difference between the total volume and total unstressed volume equal to the distending volume in each compartment. The 23 equations giving the initial conditions are listed in Appendix B. The non-linear system of 23 algebraic equations is then numerically solved to obtain the end-systolic and end-diastolic pressures for the right and left ventricles and the 19 luminal pressures for the remaining compartments (including the atria). The 19 luminal pressures and the end-diastolic left and right ventricular pressures are used to compute the initial 21 compartmental volumes which are used as initial conditions for the start of the cardiac cycle.

2.7 Concluding Remarks

The open-loop hemodynamic model described in this chapter is able to appropriately model the exposure of the cardiovascular system to various forms of orthostatic stress. Our most significant contributions to Heldt's model are the model for orthostatic stress resulting from centrifugation and the model for the collapsibility of compartments. A good check for the numerical accuracy of the simulation is to ensure the total volume over the course of an

2.7 Concluding Remarks

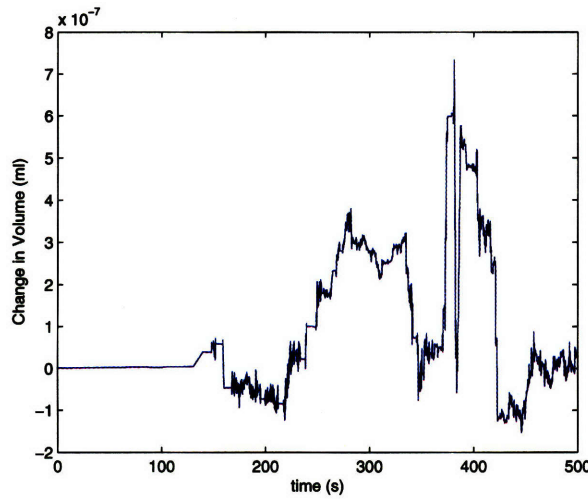


Figure 2.8: Change in total volume during a $100 \frac{\text{rev}}{\text{min}}$ centrifugation simulation.

orthostatic stress test remains conserved. Figure 2.8 plots the change in total volume over time during a centrifugation stress test at $100 \frac{\text{rev}}{\text{min}}$.

Our hemodynamic model combined with the model for the cardiovascular control system to be discussed in the following chapter is able to simulate the response of the cardiovascular system to orthostatic stress. The comparison of simulation results to experimental data will be discussed in Chapter 4.

Chapter 3

The Cardiovascular Control System

As described in Section 1.2.1, the primary function of the cardiovascular system is to deliver oxygen and nutrients and remove wastes from tissue in the human body. As such, essential to the maintenance of homeostasis is the operation of the cardiovascular system in an optimal regime, so that the exchange of chemicals with surrounding tissue occurs at an optimal rate. In order to maintain such conditions under external influences, such as orthostatic stress, built-in mechanisms exist to control cardiovascular performance, which we collectively term as the cardiovascular control system.

Cardiovascular control occurs on both a local and global level. Locally, modulation of vascular resistance in a specific region ensures that it receives adequate blood flow. Globally, overall pressure is maintained by the regulation of certain hemodynamic variables such as heart rate and cardiac contractility.

In order to appropriately simulate the response of the cardiovascular system to orthostatic stress, we must properly model the cardiovascular control system, which becomes especially relevant under conditions of stress. Our model will focus on the two major neurally-mediated reflex systems: the arterial baroreflex system and the cardiopulmonary reflex system. Figure 3.1 shows a diagrammatic representation of the cardiovascular control system. We will model these systems by combining the approaches of Heldt [2] and Samar [10].

The Cardiovascular Control System

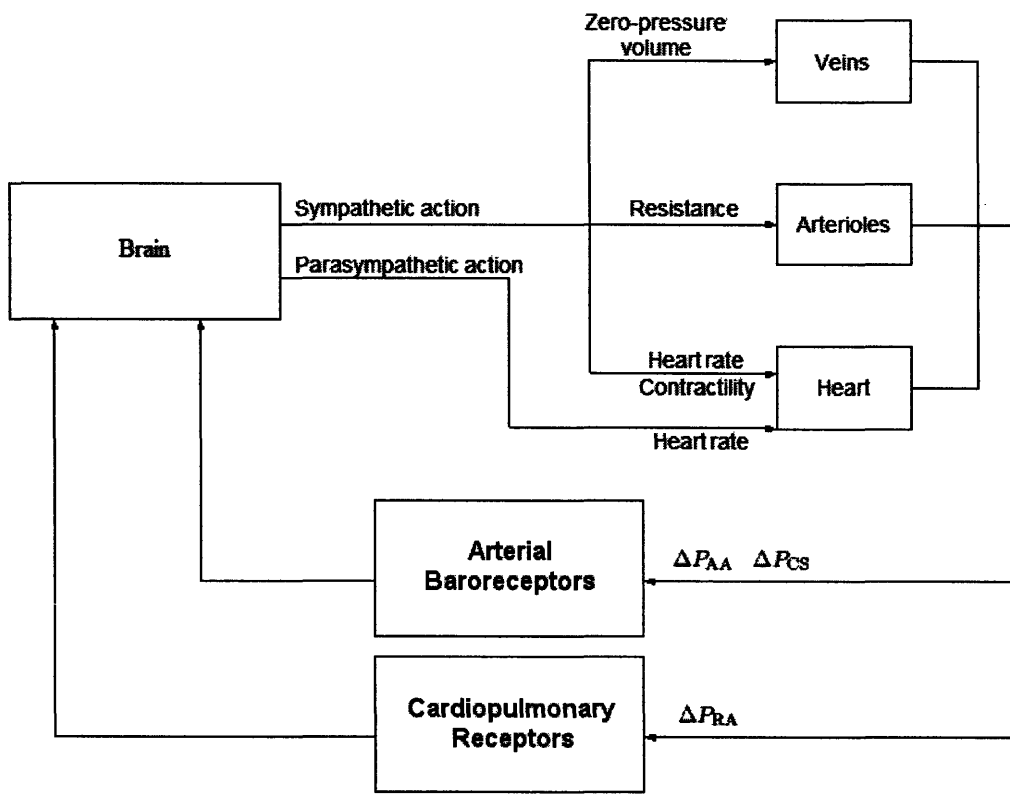


Figure 3.1: A block diagram representation of the cardiovascular control system. Modified from [10]

3.1 Arterial Baroreflex

Previous work by Davis [1] and deBoer [36] show that the arterial baroreflex system can be modeled as a negative feedback system that attempts to maintain aortic arch and carotid sinus transmural pressures at a certain set-point. As such, stretch receptors in the afferent leg of the arterial baroreflex system senses the aortic arch and carotid sinus pressures. The sensors change their rate of depolarization in response to changes in transmural pressures. The electrical impulse resulting from the depolarization (corresponding to a particular transmural pressure) travels via afferent nerve fibers to the brain, where the deviation of the transmural pressures from the set point is mapped to α -sympathetic, β -sympathetic, and parasympathetic activity in the efferent leg of the system. Increased α -sympathetic action causes a constriction of vascular smooth muscle which leads to an increase in peripheral resistance and a decrease in zero-pressure filling volume, and increased β -sympathetic action causes an increase in heart rate and cardiac contractility. An increase in parasympathetic action, on the other hand, causes heart rate to slow down.

3.1.1 Architecture

In our model, we consider a single, lumped baroreceptor whose input is the carotid sinus arterial pressure. The model for the negative feedback system subtracts the set-point pressure P_A^{sp} from the carotid sinus arterial pressure P_{CS} to produce the error signal $e_{\text{AB}}(t)$. We estimate P_{CS} in our model from the aortic arch pressure P_1 by modeling P_{CS} as being 25 cm above P_1 in a hydrostatic column, so that during centrifugation

$$e_{\text{AB}}(t) = P_1 + \frac{1}{2}\omega^2(t)(d^2 - (25 + d)^2) - P_A^{\text{sp}}$$

where, as in Section 2.4.3, d is the distance of the head from the center of rotation and $\omega(t)$ is the angular velocity of the centrifuge. Here we use a value of 91 mmHg for the set-point pressure. This error signal is subsequently fed through a non-linear mapping, in order to account for the experimentally-observed sigmoidicity of the stimulus-response curves [37]

The Cardiovascular Control System

to obtain a saturated error signal of the form

$$e_{AB}^{\text{sat}}(t) = 18 \cdot \arctan\left(\frac{e_{AB}(t)}{18}\right).$$

The saturated error signal is then taken as the input to the control system. The control system is modeled as a linear combination of two LTI filters representing the sympathetic and parasympathetic portions of the autonomic nervous system, in following with the model implemented by Samar [10]. The impulse response function of the sympathetic filter, $s(t)$, is modeled as a unit-area triangular peak and is thus parameterized in terms of three timing variables: a delay, a peak, and an end. Table 3.1 compiles the timing parameters for the sympathetic impulse response function. Using these parameters, the transfer function of

Type of Response	Delay	Peak	End
	s	s	s
Sympathetic	2	5	30

Table 3.1: Parameterization of the sympathetic impulse response function. Values taken from [10]

the sympathetic filter is written as

$$S(s) = \frac{1}{350s^2}e^{-30s} - \frac{2}{75s^2}e^{-5s} + \frac{1}{42s^2}e^{-30s}$$

The parasympathetic filter can also be modeled with a triangular impulse response, however, due to the relatively quick response of the parasympathetic limb of the reflex system, its triangular impulse response function is highly localized in time and has a delay of only one second. As Samar mentions, due to problems encountered in implementing such a filter in Simulink, the parasympathetic impulse response function can be simplified to a unit-impulse at time 0 ($p(t) = \delta(t)$), which simplifies the parasympathetic filter to the identity filter: $P(s) = 1$ [10].

The autonomic mediation of the arterial baroreflex system is executed by convolving the saturated error signal $e_{AB}^{\text{sat}}(t)$ with a linear combination of the impulse responses sym-

3.1 Arterial Baroreflex

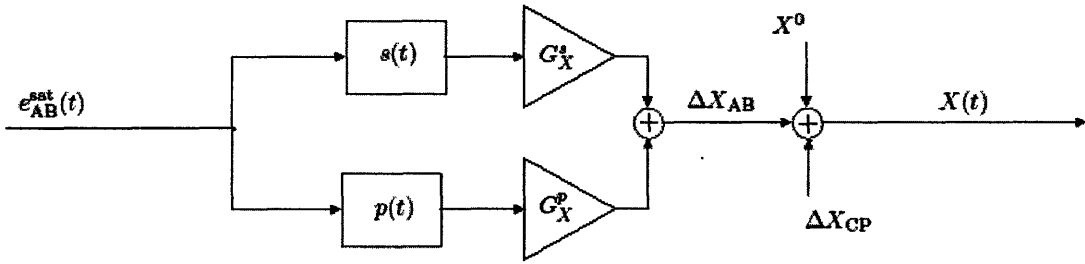


Figure 3.2: A block diagram representation of the effector mechanism for autonomic mediation.

pathetic and parasympathetic control filters to obtain ΔX , the contribution of the control system to each effector variable $X(t)$. The weights of each filter is specific to each different effector variable and are termed the as the sympathetic and parasympathetic gains for the effector variable X (G_X^s and G_X^p , respectively). The arterial baroreflex system contribution, ΔX_{AB} , is added to the cardiopulmonary reflex system contribution ΔX_{CP} , and the nominal value of the effector variable, X^0 , to obtain the value of the effector variable $X(t)$. The diagrammatic representation of our model for autonomic mediation is shown in Figure 3.2. Table 3.2 tabulates the sympathetic and parasympathetic gains for the various effector variables of the arterial baroreflex system. While the model for the control filters are taken from Samar's model [10], since the effector variables correspond the various variables in the hemodynamic model described in Chapter 2, we take the values for the gains from Heldt's model for the arterial baroreflex system [2]. Note that when the effector variable is the R-R-interval, $X(t)$ is the $I(t)$ described in the IPFM model in Section 2.3.3.

Reflex arc		G^s	G^p
R-R-interval	$\frac{\text{ms}}{\text{mmHg}}$	11	11
Left ventricular contractility	$\frac{\text{ml}}{\text{mmHg}^2}$	0.007	0
Right ventricular contractility	$\frac{\text{ml}}{\text{mmHg}^2}$	0.022	0
Arterial resistance	$\frac{\text{PRU}}{\text{mmHg}}$	-0.05	0
Venous unstressed volume	$\frac{\text{ml}}{\text{mmHg}}$	31	0

Table 3.2: Gain values for the arterial baroreflex model. Values taken from [2]

3.2 Cardiopulmonary Reflex

The afferent limb of the cardiopulmonary reflex system has cardiopulmonary receptors located in the atrio-caval junctions, the atrial walls, the ventricular walls, and the pulmonary vasculature. These sensors, typically divided into A-type mechano-receptors and B-type stretch receptors, sense changes in right atrial transmural pressure, ΔP_{RA} , and send afferent signals along vagal nerve fibers to the autonomic nervous system. Cardiopulmonary stimulation is believed to directly inhibit vasoconstrictor centers, causing reciprocal effects on parasympathetic and sympathetic outflow. Thus an increase in afferent nerve traffic corresponds to a reduction in efferent sympathetic outflow and a hypothesized increase in efferent parasympathetic outflow [2].

Our model for the cardiopulmonary reflex system will follow the same form of a negative feedback system as our model for the arterial baroreflex system, with a few important differences. Firstly, the error input is changed to

$$e_{CP}(t) = \Delta P_{RA} - P_{CP}^{sp}$$

where the set-point pressure takes a value of 5 mmHg. The non-linear mapping of the error signal leading to the saturated error signal $e_{CP}^{sat}(t)$ also is changed to

$$e_{CP}^{sat}(t) = 5 \cdot \arctan\left(\frac{e_{CP}(t)}{5}\right).$$

The saturated error signal is fed to the same sympathetic and parasympathetic control filters

described for the arterial baroreflex system, but the sympathetic and parasympathetic gains for each effector variable are different. Furthermore, the only effector variables for the model of the cardiopulmonary reflex system are arterial resistance and venous unstressed volume (we do not model the cardiopulmonary reflex system as having any direct influence on cardiac contractility or heart rate). Table 3.3 summarizes the new gain values.

Reflex arc		G^s	G^p
Arterial resistance	$\frac{\text{PRU}}{\text{mmHg}}$	0.05	0
Venous unstressed volume	$\frac{\text{ml}}{\text{mmHg}}$	100	0

Table 3.3: Gain values for the cardiopulmonary reflex model. Values taken from [2]

Given these important differences, the remaining portions of the model are identical to the model for the arterial baroreflex system. As depicted in Figure 3.2, the effect of the cardiopulmonary system on an effector variable ΔX_{CP} is added to the effect on the effector variable from the arterial baroreflex system ΔX_{AB} and the nominal value for the effector variable X^0 to obtain the complete value of the effector variable $X(t)$.

3.3 Implementation

We chose to implement our model of the cardiovascular control system in continuous time, as Simulink has a convenient method for continuous time implementation of filters in terms of their transfer functions. As the frequency response of the cardiovascular regulatory mechanism is bandlimited to frequencies less than the mean heart rate [38], it would be impractical and computationally inefficient for the cardiovascular control system to react to every sample of aortic arch, carotid sinus, and right atrial pressures. Following Samar's methodology, in order to avoid this computational inefficiency, and to attenuate the high-frequency content in the pressure signals (as they are not automatically attenuated by the model of the control system), we apply a low-pass filter to the input pressures, before they are subtracted from the set-points [10].

The Cardiovascular Control System

The sympathetic control filter, in terms of its transfer function,

$$S(s) = \frac{1}{350s^2}e^{-30s} - \frac{2}{75s^2}e^{-5s} + \frac{1}{42s^2}e^{-30s},$$

was implemented using a parallel combination of three transport delay blocks (which, acting as a pure delay, store values from previous time points in memory) each in series with a transfer function block. Such an implementation for the control system avoids having to discretize and downsample time (which avoids aliasing issues encountered in previous models by Davis and Mukkamala [1, 38]). Furthermore, it avoids the need to directly compute the convolution sum.

In our implementation, every effector variable is updated at every time step, except for the contractility variables, which are updated at the beginning of each new beat; this is because heart contractility must remain constant from beat to beat. Furthermore, the venous tone feedback, specifically to the renal veins, must be lower-bounded in order to keep the unstressed volume in that compartment greater than zero at all times.

This chapter has described our model for the cardiovascular control system. The following chapter will use simulation results to validate our model and make predictions.

Chapter 4

Model Validation and Prediction

In order to validate our model for the response of the cardiovascular system to short-radius centrifugation, we present in this chapter the comparison of our simulations to experimental data. We also compare simulations of our model with and without vessel collapsibility in order to validate our model for vessel collapse; the simulations with vessel collapsibility modeled should correct the non-physiological results seen in simulations without collapsibility modeled. Upon validation, we can use our model to predict the cardiovascular response at levels of stress that cannot yet be tested on human subjects.

4.1 Data Acquisition

Experiments were approved by MIT's Committee On the Use of Humans as Experimental Subjects (COUHES Protocol #: 0605001773) and were conducted in the Man Vehicle Laboratory of the MIT Department of Aeronautics and Astronautics under the supervision of Thomas Jarchow and Thomas Heldt. Centrifugation experiments were performed with the subject's head at the center of rotation. Seven subjects were exposed to centrifugation at low, medium, and high angular velocities (averaging 11.6 rpm, 22.9 rpm, and 29.4 rpm, respectively), with rest at zero angular velocity in between each trial to allow the cardiovascular system to return to resting conditions. Another seven subjects were exposed to two trials at high angular velocities (averaging 29.4 rpm), again with a break between the two trials. Arterial blood pressure (ABP), electrocardiogram (ECG), and strain gauge impedance signals were measured from all 14 subjects at 1000 Hz. Of these 14 subjects, ABP data were of sufficient quality in only 10 subjects; strain gauge data were only useable

Model Validation and Prediction

from 5 subjects (all of whom were exposed only to two trials at high angular velocities).

Heart rate was computed from ECG data by detecting the peak times in the ECG signal. The ECG peak times were computed using a modified version of an algorithm employed by Hastreiter [39]. The inter-beat interval, I , is the peak-to-peak interval (in seconds), and heart rate (in beats per minute) is calculated as $\text{HR} = \frac{60}{I}$. Mean arterial pressure (MAP), systolic arterial pressure (SAP), and diastolic arterial pressure (DAP) were computed by taking the average, maximum, and minimum, respectively, of the ABP signal in the inter-beat interval corresponding to each cardiac cycle. Appendix D details the code used to process the ECG and ABP data.

The strain gauge signal was used to estimate the blood volume in the legs following the methodology employed by Karemaker and colleagues [40], who maintain that the strain gauge impedance signal (Imp) is related to the volume in the legs via an affine relationship: $\text{LegVol} = A \cdot \text{Imp} + B$. The scaling factor A and the additive constant B are picked to match the strain gauge signal to the simulated volume in the lower-body compartments. As such, the strain gauge signal only conveys information about the time course of the variation of blood volume in the legs.

4.2 Model Validation

The angular velocity profiles of the 10 subjects rose from 0 to the maximum angular velocity over a period of about 40 seconds. Therefore, we simulate centrifugation in our model with the angular velocity rising over the same period. In order to compare the data to our simulations, we examine the change in the variable of interest, so that we are able to capture the response of the cardiovascular system to the stress. For all sets of data, we shift the onset time of centrifugation to 100 s, and we begin the centrifugation simulation in our model at the same time. Following the data, simulations were run at 11.6 rpm, 22.9 rpm, and 29.4 rpm. The simulations were performed without any parameter adjustments to match the simulations to the experimental data.

4.2 Model Validation

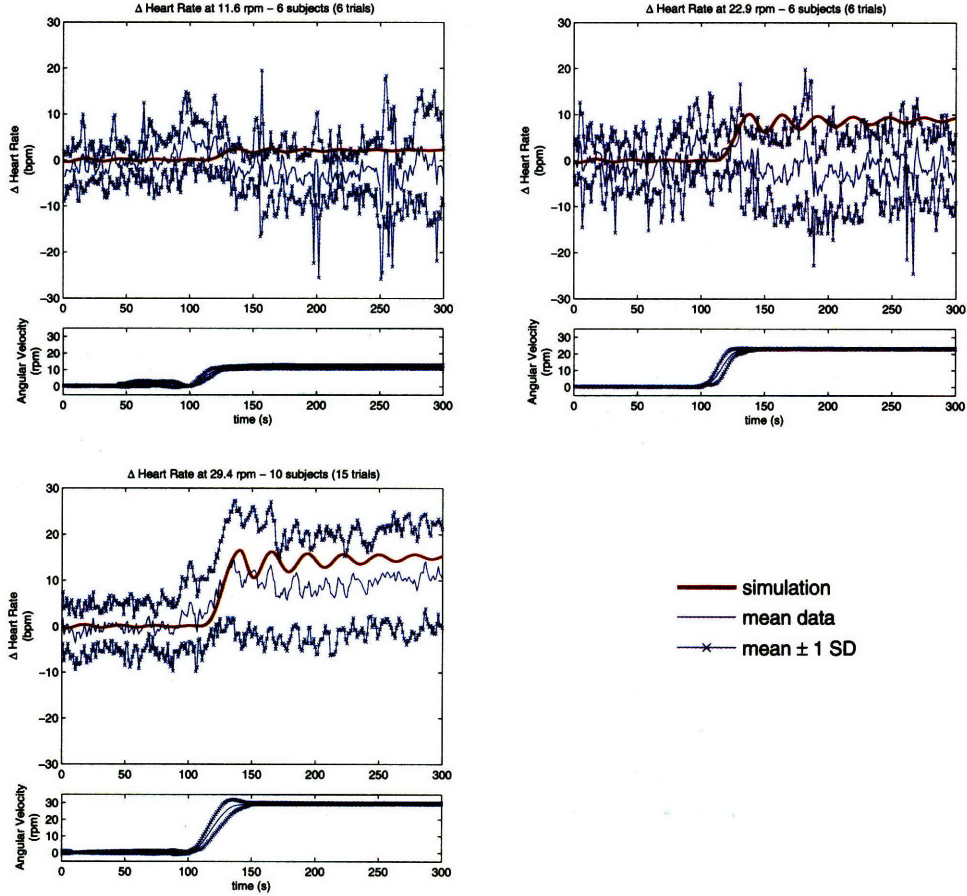


Figure 4.1: Changes in heart rate during centrifugation to 11.6 rpm (top left), 22.9 rpm (top right), and 29.4 rpm (bottom left). Heavy red line is simulated heart rate. Solid blue line is mean data and x-ed blue line is mean \pm 1 SD.

Figure 4.1 shows the response of heart rate to centrifugation at the low, medium, and high angular velocities. The simulation does remarkably well at 29.4 rpm, where the transient in the change of heart rate is almost exactly mimicked by the simulation. At both 11.6 rpm and 22.9 rpm, the simulation slightly over-estimates heart-rate from its mean value, however, in both cases the simulation still stays within one standard deviation from the mean, meaning some subjects did exhibit the heart rate response predicted by the model at these angular velocities.

The response of mean arterial pressure to centrifugation at the three angular veloci-

Model Validation and Prediction

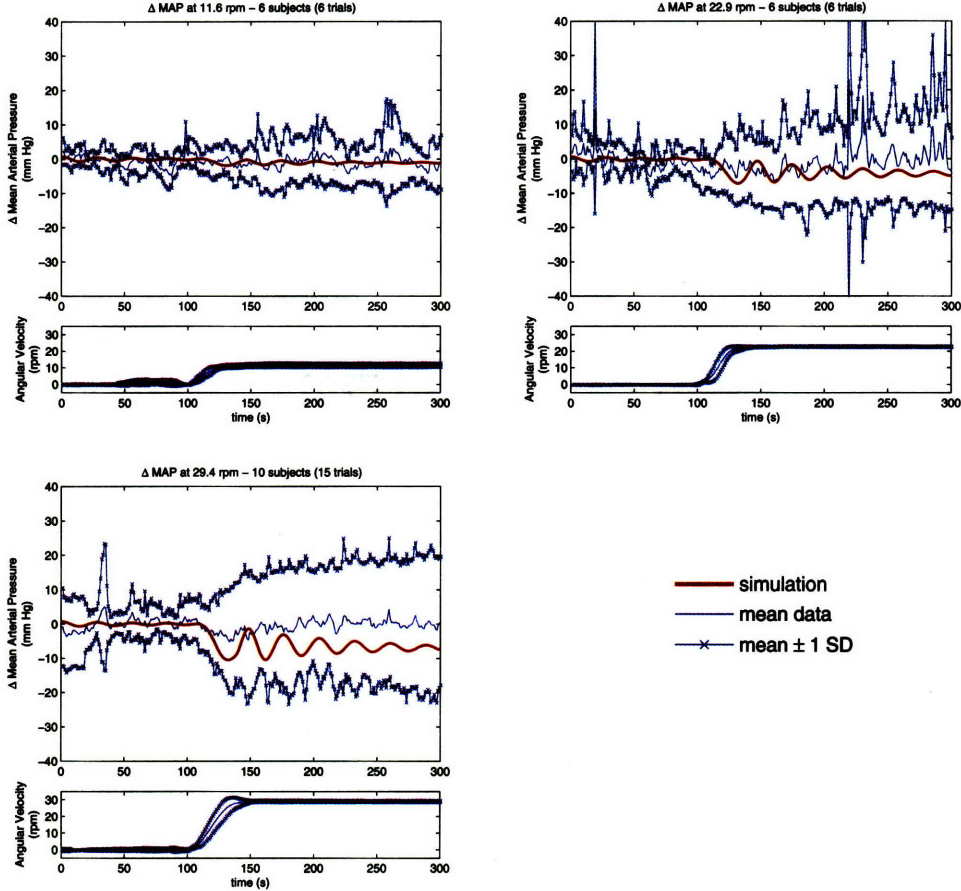


Figure 4.2: Changes in mean arterial pressure during centrifugation to 11.6 rpm (top left), 22.9 rpm (top right), and 29.4 rpm (bottom left). Heavy red line is simulated MAP. Solid blue line is mean data and x-ed blue line is mean \pm 1 SD.

ties is depicted in Figure 4.2. Our model does quite well at 11.6 rpm and 22.9 rpm, closely following the mean data throughout the simulation. (The peaks in the 22.9 rpm MAP data occurring around 220 s result from artifacts in the ABP data.) At 29.4 rpm, the simulation slightly underestimates MAP, however, it still falls well within one standard deviation from the mean.

Figure 4.3 depicts the response of systolic arterial pressure to orthostatic stress resulting from centrifugation. As with MAP, our model does very well in predicting the response of SAP to centrifugation at 11.6 rpm and 22.9 rpm. Again, we also see the same

4.2 Model Validation

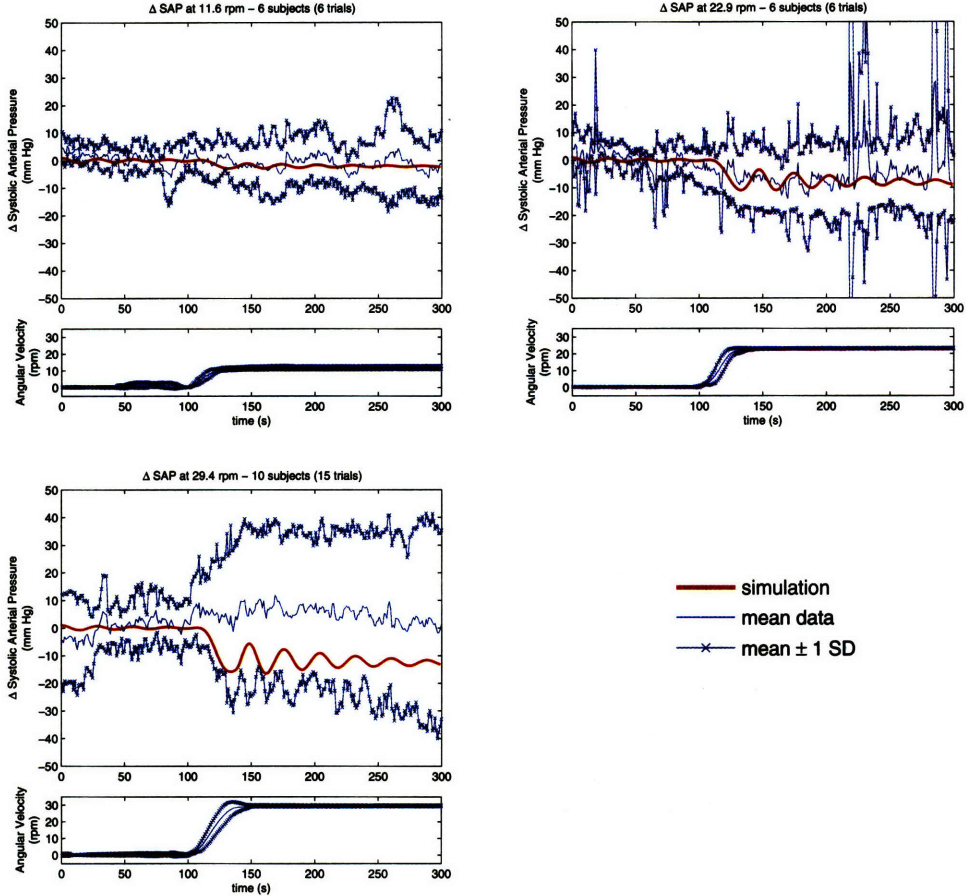


Figure 4.3: Changes in systolic arterial pressure during centrifugation to 11.6 rpm (top left), 22.9 rpm (top right), and 29.4 rpm (bottom left). Heavy red line is simulated SAP. Solid blue line is mean data and x-ed blue line is mean \pm 1 SD.

artifact in the SAP data at around 220 s as well as another artifact near 290 s. As we found with MAP, the model underestimates SAP at 29.4 rpm, this time underestimating by about 15 mmHg. However, in spite of the larger amount by which SAP is underestimated, as before, the simulation still falls within one standard deviation from the mean. In fact, the experimental data has a relatively high standard deviation of around 40 mmHg, which means that the response of SAP is highly variable from subject to subject.

The plots of the response of diastolic arterial pressure to centrifugation, shown in Figure 4.4, show a very nice correlation between our model and the experimental data.

Model Validation and Prediction

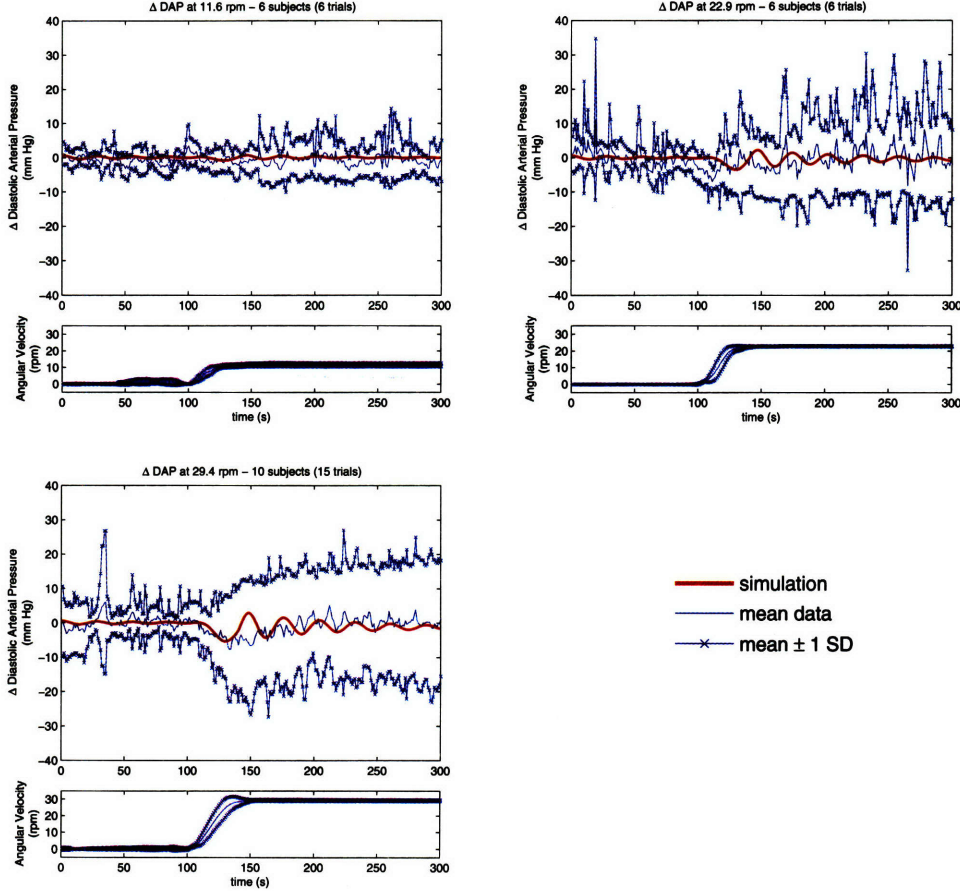


Figure 4.4: Changes in diastolic arterial pressure during centrifugation to 11.6 rpm (top left), 22.9 rpm (top right), and 29.4 rpm (bottom left). Heavy red line is simulated DAP. Solid blue line is mean data and x-ed blue line is mean ± 1 SD.

At all three angular velocities, the simulated DAP falls nearly exactly in line with the mean data. At 29.4 rpm, the model even captures the transient from baseline to (cyclic) steady-state.

As we mentioned in the previous section, the strain gauge data was only useable for 5 subjects, each of whom were only subject to two trials of 29.4 rpm centrifugation. Figure 4.5 shows the response of the volume in the legs (estimated from the strain gauge data). In order to pick the constants A and B for each subject in the relation $\text{LegVol} = A \cdot \text{Imp} + B$, first the baseline volume for each subject is matched to the simulation baseline leg volume,

4.2 Model Validation

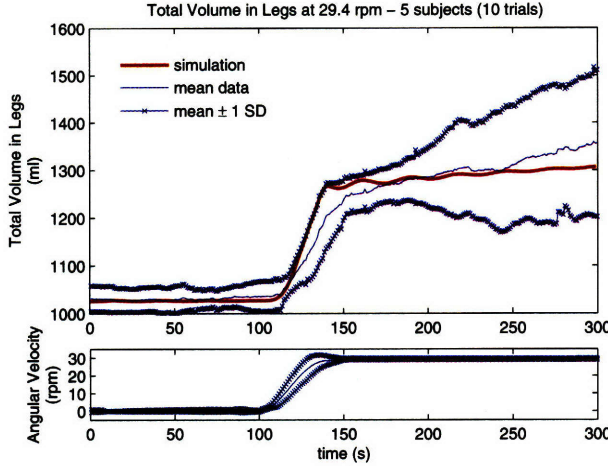


Figure 4.5: Changes in leg volume during centrifugation to 29.4 rpm. Heavy red line is simulated leg volume. Solid blue line is mean data and x-ed blue line is mean \pm 1 SD.

and subsequently the volume at the point at which the slope of the strain gauge data changes is set to the simulated volume at the corresponding point. As discussed, since the strain gauge data is scaled to match the simulated leg volume, the only information conveyed by this data is from the shape of the transient, which allows for understanding the time course of the variation of blood volume in the legs. Upon examination of Figure 4.5, we see that the simulated leg volume rises significantly faster than the mean of the data. However, the simulation still stays just within the range of one standard deviation from the mean. A reason for our simulation over-estimating the rate of change of leg volume may be due to a physiological phenomenon known as venous stress-relaxation [40], which was not incorporated into our model. In short, venous stress-relaxation is the tending of vessels to, upon a rise in transmural pressure, ‘stress’ by initially keeping their volume relatively constant, and then ‘relax’ by allowing volume to increase according to the normal pressure-volume relation (see Chapter 2).

We have shown in this section that our simulation results for arterial blood pressure, heart rate, and leg volume match the experimental data quite well. The simulated response of the cardiovascular system to centrifugation follows the mean data very closely for most variables of interest, and stays within one standard deviation from the mean for all variables

Model Validation and Prediction

of interest.

4.3 Prediction with Centrifugation Simulations

Having validated our model for the response of the cardiovascular system to short-radius centrifugation in the previous section, we proceed in this section to use our model to make predictions about the cardiovascular response to centrifugation over a large range of angular velocities. In order to understand the significance of vessel collapse, we ran simulations both with and without the collapsibility of vessels modeled.

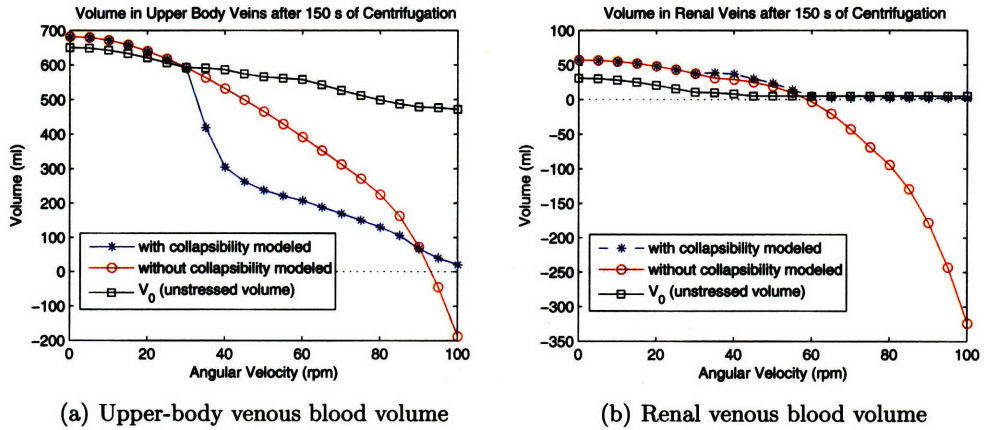


Figure 4.6: Simulated response of blood volume in the upper-body and renal veins after 150 s of centrifugation. The black dotted line is at zero volume. In both figures, the simulations with collapsibility modeled do not allow volume to become negative.

In Figure 4.6, the simulated volumes in the upper-body and renal veins after 150 s of centrifugation are plotted over a range of angular velocities. We choose to plot the volumes in these compartments as they both exhibit vessel collapse at reasonably high levels of stress (according to our simulations). We observe that for both compartments, the simulation with collapsibility modeled does not allow the compartmental volume to drop below zero; such is not the case for the simulation without collapsibility modeled, in which the volume falls far below zero at high levels of stress in both compartments (a completely non-physiological response, as vessel volume is always nonnegative). Furthermore, while the compartmental

4.3 Prediction with Centrifugation Simulations

volume is above the unstressed volume, there should be very little difference between the two models, and, as we expect, the compartmental volumes are nearly equal in this range. In both compartments, a significant difference is seen only after the vascular volumes fall below the unstressed volume.

Having shown that our model for vessel collapse does indeed keep compartmental volume from falling into negative ranges, even at exceedingly high levels of stress, we now turn our attention to predicting the response of important physiological variables, namely mean, systolic, and diastolic arterial pressures, heart rate, blood volume in the legs, cardiac output, total peripheral resistance, and stroke volume.

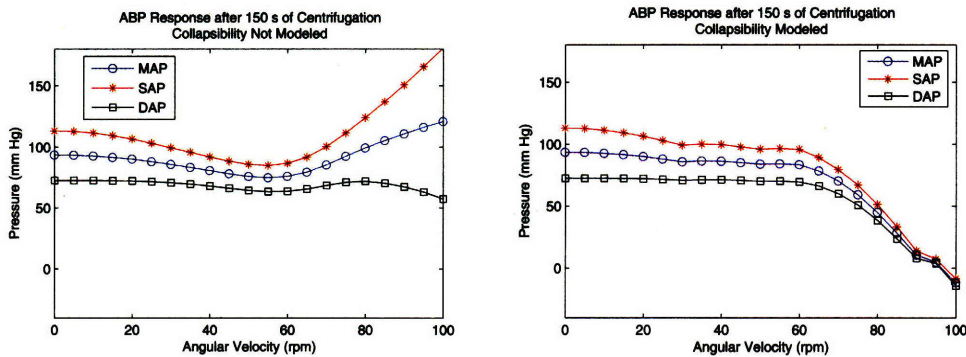


Figure 4.7: Simulated response of mean arterial pressure, systolic arterial pressure, and diastolic arterial pressure after 150 s of centrifugation. The model with vessel collapsibility corrects the unexpected recovery of ABP seen in the simulations without collapsibility modeled.

The simulated responses of mean, systolic, and diastolic arterial pressures are shown in Figure 4.7. In the simulation with vessel collapse modeled, we observe that all three blood pressures drop slightly until 30 rpm, where they are maintained at their lower values until about 60 rpm, at which point the cardiovascular control mechanisms are no longer able to maintain arterial blood pressure, and the pressures drop significantly to physiologically hazardous levels. A fourth region of behavior is observed after 90 rpm. The differences in the cardiovascular response in these four regions are explained by the occurrence of vessel collapse at the boundaries of each region. The simulations show the upper-body veins collapsing at angular velocities above 30 rpm, the superior vena cava, abdominal veins,

Model Validation and Prediction

and renal veins collapsing after 55-60 rpm, and the upper-body arteries collapsing after 90-95 rpm. The simulations without vessel collapse modeled show a similar behavior at angular velocities under 60 rpm, but as the angular velocity increases above this point, we see a counter-intuitive recovery of MAP and SAP, due to the model allowing certain compartmental volumes to become negative, effectively injecting volume into the circulation.

Figure 4.8 shows a similar relationship between the two models in the response to heart rate. The simulations with vessel collapse modeled show heart rate continuing to increase in order to compensate for the increasingly higher levels of stress, whereas without vessel collapse modeled, the simulations show a physiologically unexpected recovery of heart rate at angular velocities above 60 rpm. Again, in the model with vessel collapse, we observe four regions of distinct cardiovascular responses occurring at the same angular velocities mentioned previously.

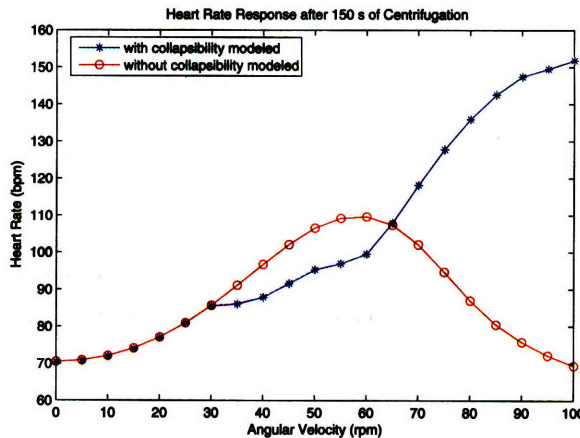


Figure 4.8: Simulated response of heart rate after 150 s of centrifugation. The model with vessel collapsibility corrects the unexpected recovery of heart rate seen in the simulation without collapsibility modeled.

Figure 4.9 plots the simulated response of blood volume in the legs to centrifugation. As we expect, the blood volume in the legs increases monotonically with increasing stress. We find that the simulations without vessel collapse modeled actually show a greater increase in leg blood volume. This is due to the injection of volume into the cardiovascular system when certain compartmental volumes enter negative regimes.

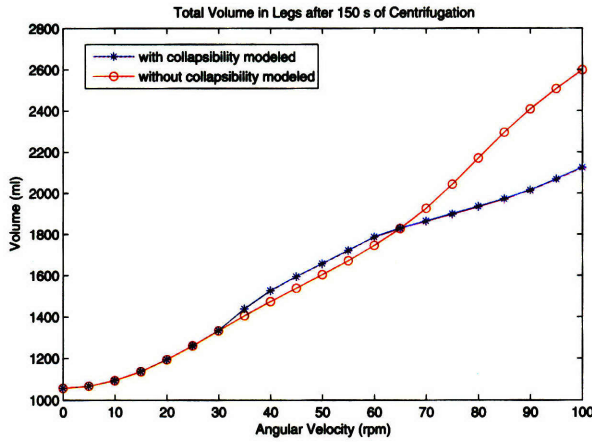


Figure 4.9: Simulated response of blood volume in the legs after 150 s of centrifugation. The simulation without vessel collapse modeled shows a higher leg volume due to the (non-physiological) injection of volume into the circulation from compartments with negative volumes.

The simulated responses (with vessel collapse modeled) of cardiac output, stroke volume, and total peripheral resistance are plotted in Figure 4.10. We observe an overall decrease in cardiac output and stroke volume and an increase in total peripheral resistance with increasing levels of orthostatic stress. We notice that the decrease in cardiac output and stroke volume is steady until about 30 rpm, followed by a maintenance phase between 30 and 55 rpm, after which point their values fall steeply. A same pattern is seen in the increase of total peripheral resistance, however, we observe a jump of around 0.5 PRU after 95 rpm. Again, these regions of different cardiovascular response are explained by the simulated collapse of vascular compartments occurring at the angular velocities at which the response changes.

4.4 Summary

In this chapter, we have shown that our model for the response of the cardiovascular system to centrifugation compares well to experimental data. Furthermore, we have demonstrated the ability of the model to predict the response of the cardiovascular system at levels

Model Validation and Prediction

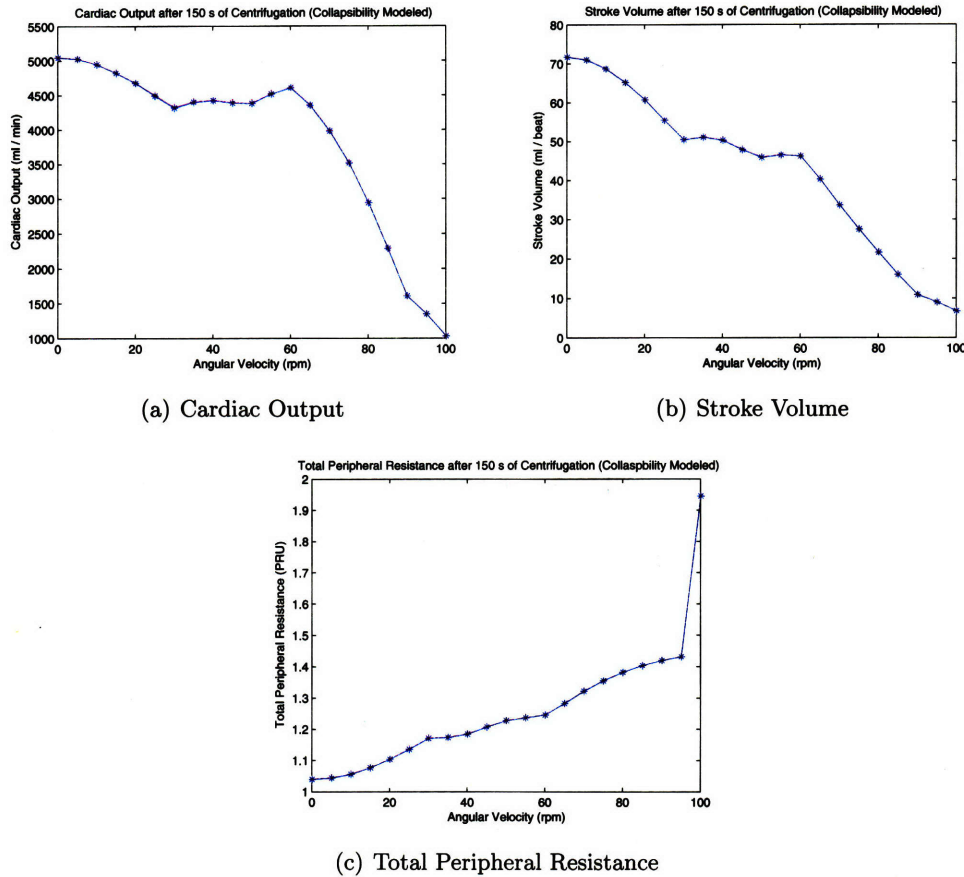


Figure 4.10: Simulated response of cardiac output, stroke volume, and total peripheral resistance after 150 s of centrifugation.

of stress that are too high to be tested on human subjects on a short-radius centrifuge. Moreover, these predictions have validated and shown the significance of our model for the collapsibility of blood vessels discussed in Section 2.5.

Chapter 5

Conclusions and Recommendations for Future Work

In this thesis, we developed a mathematical model for simulating the cardiovascular response to short-radius centrifugation and have shown its predictions to be consistent with experimental data. Short-radius centrifugation is an important and efficient measure against cardiovascular deconditioning during spaceflight. Therefore, it is important to understand the response of the cardiovascular system to short-radius centrifugation, which is greatly aided by the model presented in this work. The work in this thesis was divided into three portions: (1) developing the mathematical model for cardiovascular response to centrifugation, (2) validating our model against experimental data, and (3) using our model to make predictions about the response of the cardiovascular system under high levels of centrifugal acceleration.

Below we summarize the work presented in the thesis and make suggestions for future work that can build off of our efforts.

5.1 Summary

In Chapter 2, we outlined our construction of the hemodynamic model for the cardiovascular response to centrifugation. We built our model starting with an existing 21-compartment hemodynamic model developed by Heldt [2]. Our primary additions to Heldt’s model were incorporating a framework for simulation of the hydrostatic pressure resulting from centrifugal acceleration and developing and integrating a numerically feasible model for the

Conclusions and Recommendations for Future Work

collapsibility of blood vessels. Modeling of the flow through a collapsible vessel can effectively be viewed as a continuous implementation of the idealized Starling resistor [31,32]. We modeled the pressure-volume relation of a collapsible vessel using a piecewise-linear model approximately fit to experimental data. Our hemodynamic model was built in Simulink, using the code from a previous six-compartment model built by Samar [10] as the skeleton for our code.

In Chapter 3, we discussed the model for the cardiovascular control system. Our model for the control system combined previous work by Heldt [2] and Samar [10]. The control system consisted of two reflex loops: the arterial baroreflex and the cardiopulmonary reflex. Each reflex loop was modeled as a set-point controller with the baroreflex system sensing carotid sinus arterial pressure and the cardiopulmonary reflex sensing right atrial transmural pressure. On the efferent limb, the baroreflex system exerts both sympathetic and parasympathetic control, while the cardiopulmonary system exerts only sympathetic control.

In Chapter 4, we validated our simulations against experimental data and used our model to predict the response of the cardiovascular system to extreme levels of centrifugal stress. We found that our simulation results closely matched the experimental data; in all cases the simulation stayed within one standard error from the mean, and in many cases followed the mean quite closely. Furthermore, our predictions also served to validate our model for vessel collapse, as a significant difference was seen between simulations with and without vessel collapse modeled; most notably, the simulations with vessel collapse modeled never allowed any compartmental volume to fall below zero. Our predictions showed a failure of the cardiovascular system to control mean arterial pressure at angular velocities exceeding 60 rpm, at which point the mean arterial pressure begins to fall to physiologically hazardous levels.

5.2 Recommendations for Future Work

We suggest the following avenues for future work based on our research:

Allometry of the Cardiovascular System The parameters listed for our model in Chapters 2 and 3 were designed for the cardiovascular system of a healthy 169 cm, 70 kg individual. According to Heldt [2], as subjects vary in weight, height, and other anthropometric measures, the parameters profiles associated with the model should also change according to allometric scaling laws. Various mathematical models for establishing the dependence of each cardiovascular parameter on anthropometric parameters [41–43] can be employed to tune our model to the cardiovascular system of each specific subject. This will allow for a much more accurate prediction of the response of the cardiovascular system of a specific subject to centrifugal acceleration.

Optimization of the Centrifugal Stress Test An overall aim of our model is to understand the response of the cardiovascular system to centrifugal acceleration so that centrifugation can be used as an appropriate counter-measure to cardiovascular deconditioning during spaceflight. As such, it is desirable to know exactly what angular velocity profile can best simulate 1 G conditions. Our simulations can be compared to the cardiovascular response to standard gravitational stress tests, such as upright tilt and stand-up tests, in order to find the optimal angular velocity profile which best simulates 1 G conditions.

Appendix A

Analytical Solutions to Interstitial Fluid Flow and Volume

The analytical solutions to the transcapillary flow and volume discussed in Section 2.4.1 are broken into four regions and given below. The equations, taken from Heldt [2], are:

Region I: Gradual increase in orthostatic stress over a period of length Δt .

$$q(t) = \frac{V_{max}}{\Delta t} \cdot \left(1 - e^{-\frac{t}{\tau}}\right) \quad (\text{A.1})$$

$$V(t) = V_{max} \cdot \left(\frac{t}{\Delta t} - \frac{\tau}{\Delta t} \left(1 - e^{-\frac{t}{\tau}}\right)\right) \quad (\text{A.2})$$

Region II: Full orthostatic stress during period of duration T_{tilt} .

$$q(t) = \frac{V_{max}}{\Delta t} \cdot \left(1 - e^{-\frac{\Delta t}{\tau}}\right) \cdot e^{-\frac{t-\Delta t}{\tau}} \quad (\text{A.3})$$

$$V(t) = V_{max} \cdot \left(1 - \frac{\tau}{\Delta t} \left(1 - e^{-\frac{\Delta t}{\tau}}\right) e^{-\frac{t-\Delta t}{\tau}}\right) \quad (\text{A.4})$$

Region III: Gradual decline in orthostatic stress over a period of length Δt .

$$q(t) = \frac{V_{max}}{\Delta t} \cdot \left(1 + \left(1 - e^{-\frac{\Delta t}{\tau}}\right) e^{-\frac{T_{tilt}}{\tau}}\right) \cdot e^{-\frac{t-(\Delta t+T_{tilt})}{\tau}} - \frac{V_{max}}{\delta t} \quad (\text{A.5})$$

$$\begin{aligned} V(t) &= V_{max} \cdot \left(1 - \frac{t - (\Delta t + T_{tilt})}{\Delta t}\right) - V_{max} \cdot \frac{\tau}{\Delta t} \cdot \left(1 - e^{-\frac{\Delta t}{\tau}}\right) \cdot e^{-\frac{T_{tilt}}{\tau}} + \\ &\quad + V_{max} \cdot \frac{\tau}{\Delta t} \cdot \left(1 + \left(1 - e^{-\frac{\Delta t}{\tau}}\right) e^{-\frac{T_{tilt}}{\tau}}\right) \cdot \left(1 - e^{-\frac{t-(\Delta t+T_{tilt})}{\tau}}\right) \end{aligned} \quad (\text{A.6})$$

Analytical Solutions to Interstitial Fluid Flow and Volume

Region IV: Post-orthostatic stress recovery of unspecified length.

$$q(t) = -\frac{V_{max}}{\Delta t} \cdot \left(1 - e^{-\frac{\Delta t}{\tau}}\right) \cdot \left(1 - e^{-\frac{T_{tilt} + \Delta t}{\tau}}\right) \cdot e^{-\frac{t-(2\Delta t + T_{tilt})}{\tau}} \quad (\text{A.7})$$

$$V(t) = V_{max} \cdot \frac{\tau}{\Delta t} \cdot \left(1 - e^{-\frac{\Delta t}{\tau}}\right) \cdot \left(1 - e^{-\frac{T_{tilt} + \Delta t}{\tau}}\right) \cdot e^{-\frac{t-(2\Delta t + T_{tilt})}{\tau}} \quad (\text{A.8})$$

Here T_{tilt} is the time during which the tilt angle remains at α_{max} . The parameters τ and V_{max} depend on the nature of the orthostatic stress and are discussed in Section 2.4.

Appendix B

Method for Finding Initial Conditions to Hemodynamic Model

As discussed in Section 2.6.4, the initial conditions for the state variables of the hemodynamic model are obtained by implementing a modified version of the method used by Davis to solve for the initial conditions of his six compartment model [1]. By equating the right ventricular stroke volume and left ventricular stroke volume, and deriving equations for the average blood passing through the remaining compartments under the assumption that the capacitors are not conducting, we form a system of 22 linear algebraic equations (in the luminal pressures and end-systolic and end-diastolic left and right ventricular pressures). A 23rd non-linear equation is obtained on the basis of conservation of volume, setting the difference between the total volume and total unstressed volume equal to the distending volume in each compartment. The 23 equations giving the initial conditions are given below:

$$C_{\text{lv}}^{\text{ed}} \cdot (P_{\text{lv}}^{\text{ed}} - P_{\text{th}}) - C_{\text{lv}}^{\text{es}} \cdot (P_{\text{lv}}^{\text{es}} - P_{\text{th}}) = C_{\text{rv}}^{\text{ed}} \cdot (P_{\text{rv}}^{\text{ed}} - P_{\text{th}}) - C_{\text{rv}}^{\text{es}} \cdot (P_{\text{rv}}^{\text{es}} - P_{\text{th}}) \quad (\text{B.1})$$

$$C_{\text{rv}}^{\text{ed}} \cdot (P_{\text{rv}}^{\text{ed}} - P_{\text{th}}) - C_{\text{rv}}^{\text{es}} \cdot (P_{\text{rv}}^{\text{es}} - P_{\text{th}}) = T_s^v \cdot \frac{P_{\text{lv}}^{\text{es}}}{R_1} \quad (\text{B.2})$$

$$T_s^v \cdot \frac{P_{\text{lv}}^{\text{es}}}{R_1} = I_0 \cdot \left(\frac{P_1 - P_2}{R_2} + \frac{P_1 - P_6}{R_6} \right) \quad (\text{B.3})$$

$$I_0 \cdot \frac{P_1 - P_2}{R_2} = I_0 \cdot \frac{P_2 - P_3}{R_3} \quad (\text{B.4})$$

$$I_0 \cdot \frac{P_2 - P_3}{R_3} = I_0 \cdot \frac{P_3 - P_4}{R_{\text{ub}}} \quad (\text{B.5})$$

$$I_0 \cdot \frac{P_3 - P_4}{R_{\text{ub}}} = I_0 \cdot \frac{P_4 - P_5}{R_4} \quad (\text{B.6})$$

$$I_0 \cdot \frac{P_4 - P_5}{R_4} = I_0 \cdot \frac{P_5 - P_{\text{ra}}}{R_5} \quad (\text{B.7})$$

$$I_0 \cdot \frac{P_1 - P_6}{R_6} = I_0 \cdot \frac{P_6 - P_7}{R_7} \quad (\text{B.8})$$

$$I_0 \cdot \frac{P_6 - P_7}{R_7} = I_0 \cdot \left(\frac{P_7 - P_8}{R_8} + \frac{P_7 - P_{10}}{R_{10}} + I_0 \cdot \frac{P_7 - P_{12}}{R_{12}} \right) \quad (\text{B.9})$$

$$I_0 \cdot \frac{P_7 - P_8}{R_8} = I_0 \cdot \frac{P_8 - P_9}{R_{\text{rc}}} \quad (\text{B.10})$$

$$I_0 \cdot \frac{P_8 - P_9}{R_{\text{rc}}} = I_0 \cdot \frac{P_9 - P_{14}}{R_9} \quad (\text{B.11})$$

$$I_0 \cdot \frac{P_7 - P_{10}}{R_{10}} = I_0 \cdot \frac{P_{10} - P_{11}}{R_{\text{sc}}} \quad (\text{B.12})$$

$$I_0 \cdot \frac{P_{10} - P_{11}}{R_{\text{sc}}} = I_0 \cdot \frac{P_{11} - P_{14}}{R_{11}} \quad (\text{B.13})$$

$$I_0 \cdot \frac{P_7 - P_{12}}{R_{12}} = I_0 \cdot \frac{P_{12} - P_{13}}{R_{\text{lc}}} \quad (\text{B.14})$$

$$I_0 \cdot \frac{P_{12} - P_{13}}{R_{\text{lc}}} = I_0 \cdot \frac{P_{13} - P_{14}}{R_{13}} \quad (\text{B.15})$$

$$I_0 \cdot \left(\frac{P_9 - P_{14}}{R_9} + \frac{P_{11} - P_{14}}{R_{11}} + \frac{P_{13} - P_{14}}{R_{13}} \right) = I_0 \cdot \frac{P_{14} - P_{15}}{R_{14}} \quad (\text{B.16})$$

$$I_0 \cdot \frac{P_{14} - P_{15}}{R_{14}} = I_0 \cdot \frac{P_{15} - P_{\text{ra}}}{R_{15}} \quad (\text{B.17})$$

$$I_0 \cdot \left(\frac{P_5 - P_{\text{ra}}}{R_5} + \frac{P_{15} - P_{\text{ra}}}{R_{15}} \right) = T_d^v \cdot \frac{P_{\text{ra}} - P_{\text{rv}}^{\text{ed}}}{R_{\text{tri}}} \quad (\text{B.18})$$

$$T_d^v \cdot \frac{P_{\text{ra}} - P_{\text{rv}}^{\text{ed}}}{R_{\text{tri}}} = T_s^v \cdot \frac{P_{\text{rv}}^{\text{ed}} - P_{\text{pa}}}{R_{\text{pa}}} \quad (\text{B.19})$$

$$T_s^v \cdot \frac{P_{\text{rv}}^{\text{ed}} - P_{\text{pa}}}{R_{\text{pa}}} = I_0 \cdot \frac{P_{\text{pa}} - P_{\text{pv}}}{R_p} \quad (\text{B.20})$$

$$I_0 \cdot \frac{P_{\text{pa}} - P_{\text{pv}}}{R_p} = I_0 \cdot \frac{P_{\text{pv}} - P_{\text{la}}}{R_{\text{pv}}} \quad (\text{B.21})$$

$$I_0 \cdot \frac{P_{\text{pv}} - P_{\text{la}}}{R_{\text{pv}}} = T_d^v \cdot \frac{P_{\text{la}} - P_{\text{lv}}^{\text{ed}}}{R_{\text{mitral}}} \quad (\text{B.22})$$

$$V_{\text{total}} - V_{\text{total}}^0 = \sum_{j \in \left\{ \begin{array}{l} 1, 2, \dots, 10, \\ 12, 15, ra, rv, \\ pa, pv, la, lv \end{array} \right\}} C_j \cdot \Delta P_j + \sum_{k \in \{11, 13, 14\}} \left[\frac{2V_{\max k}}{\pi} \cdot \arctan \left(\frac{\pi C_{0k}}{2V_{\max k}} \cdot \Delta P_k \right) \right] \quad (\text{B.23})$$

This non-linear system of 23 algebraic equations is then numerically solved to obtain the end-systolic and end-diastolic pressures for the right and left ventricles and the 19 luminal pressures for the remaining compartments (including the atria). The 19 luminal pressures and the end-diastolic left and right ventricular pressures are used to compute the initial 21 compartmental volumes which are used as initial conditions for the start of the cardiac cycle.

Appendix C

Description of Simulink and MATLAB Code for the Cardiovascular Model

As discussed in Sections 2.6 and 3.3, we implemented our model in Simulink, using a previous six-compartment model developed by Samar [10] as the skeleton for our code. To ease with understanding the design of our code, we present a schematic for the layout of our code in Figure C.1. It is important to understand that the schematic does not represent the algorithmic flow of the code; rather, each block represents the subsystems responsible for computing certain variables (such as the compartmental flow rates, the orthostatic stress inputs, or the arterial baroreflex control action). Expanding each block in Figure C.1 appropriately gives the Simulink code we used to implement our model in Figure C.2. The subsystems in Figure C.2 are not shown here; instead, we briefly detail the inter-workings of our code and list the code outputs in terms of the model variables described in Chapters 2 and 3.

Briefly expanding on the notation used in our code, the variables P_1 to P_{15} , V_1 to V_{15} , and dV_1 to dV_{15} refer to the 15 compartmental luminal pressures, compartmental volumes, and the time derivatives of the volumes, respectively. P_l , P_r , P_{la} , and P_{ra} refer to the left and right ventricular and left and right atrial pressures, respectively, and V_l , V_r , V_{la} , V_{ra} , dV_l , dV_r , dV_{la} , and dV_{ra} refer to the respective cardiac volumes and their time derivatives. P_{pa} and P_{pv} refer to the pulmonary arterial and venous pressures, respectively, and V_{pa} , V_{pv} , dV_{pa} , and dV_{pv} refer to the respective pulmonary compartmental blood volumes and their time derivatives. The variable HR does not refer to the heart rate, but to the inter-beat interval. For compartment i , the variables q_{i_in} and q_{i_out} refer to the volumetric flow

Description of Simulink and MATLAB Code for the Cardiovascular Model

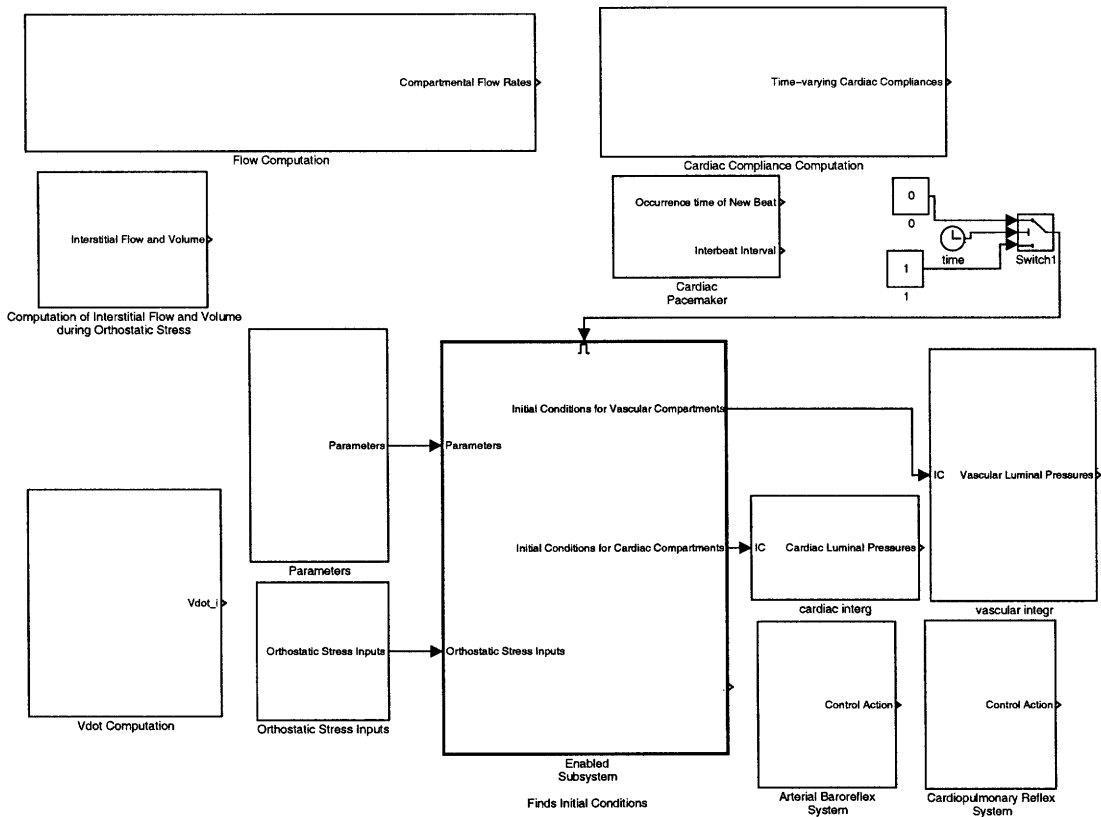


Figure C.1: Schematic drawing for the layout of the code for the cardiovascular model.

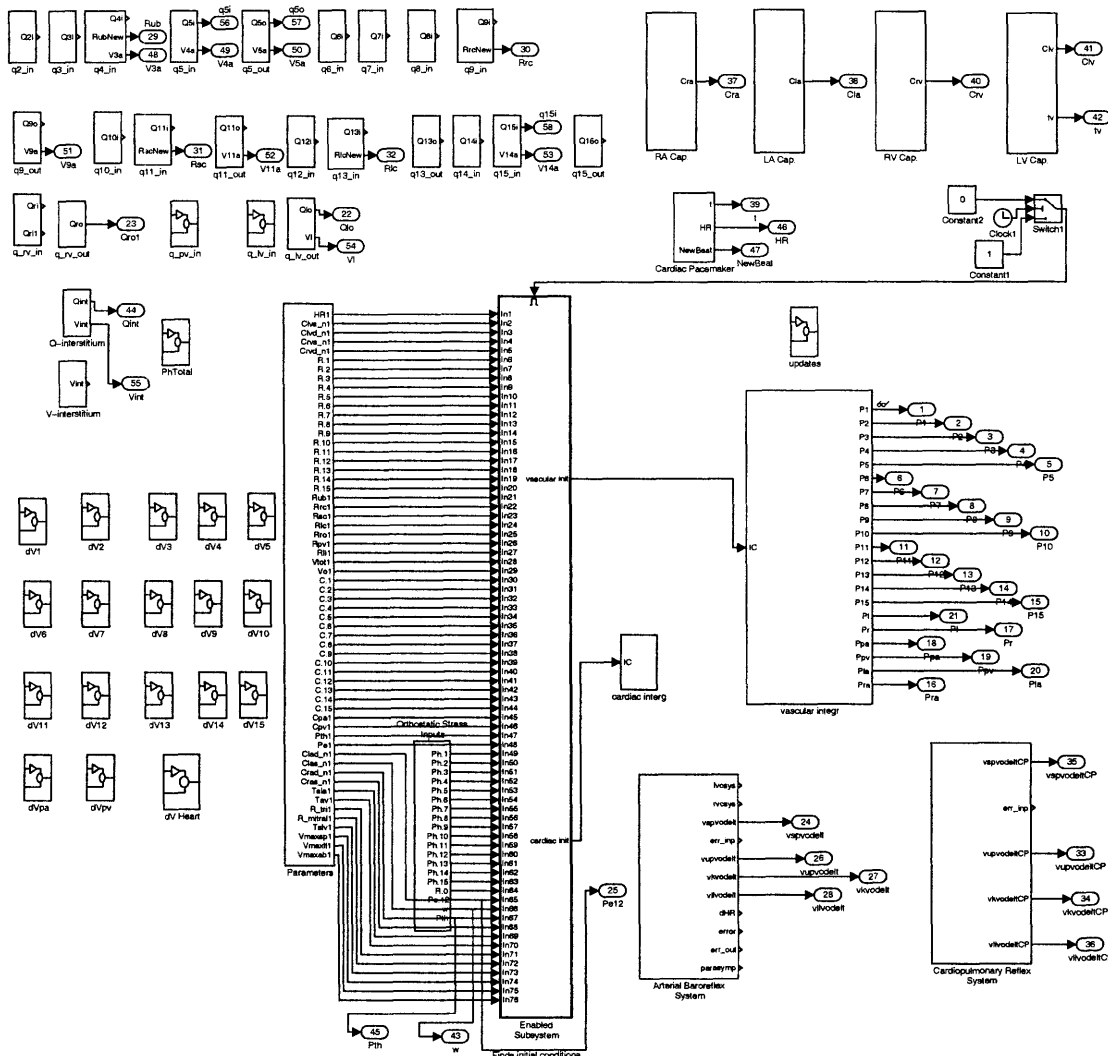


Figure C.2: Actual Simulink code used for the cardiovascular model.

Description of Simulink and MATLAB Code for the Cardiovascular Model

rate into and out of the compartment. Likewise, the variables C_i refer to the compliance of compartment i .

Having described the most essential variables in the code, we briefly explain the structure of our code. The **Parameters** subsystem sets the nominal parameters of the hemodynamic model (see Chapter 2 for the values), and the **Orthostatic Stress Inputs** subsystem sets the time-varying hydrostatic pressures and other model inputs resulting from orthostatic stress. These parameters and inputs are fed to the **Enabled Subsystem** block, which, using the methodology described in Appendix B, sets the initial conditions for the state variables. The initial conditions are fed to the **vascular integr** and **cardiac integr** subsystems, which perform the integration (according to the `ode23t` numerical solver) to give the values of the state variables at the current time step. The subsystems in the upper-left portion of the code compute the compartmental flow rates at each time step as a function of the state variables. The blocks labeled **RA Cap.**, **LA Cap.**, **RV Cap.**, and **LV Cap.** in the upper-right portion of the code compute time-varying cardiac compliances. The subsystem beneath these labeled **Cardiac Pacemaker** implements the model of the cardiac pacemaker to compute the times at which a new beat occurs as well as the inter-beat interval. The subsystems labeled **dV1** to **dV Heart** in the lower-left portion of the model compute the variables dV_i (the time-derivative of the volume for compartment i), which are subsequently fed to the **vascular integr** and **cardiac integr** subsystems to be integrated. The subsystems in the lower-right portion of the code called **Arterial Baroreflex System** and **Cardiopulmonary Reflex System** represent the arterial baroreflex and cardiopulmonary reflex systems, respectively. They take as inputs **P1** and **(Pra-Pth)**, respectively, and output control actions, which are added to the controlled cardiovascular parameters.

The outputs of the code are **tout**, a column vector of time points, and **yout**, a 58 column matrix with rows corresponding to the time points in **tout** and each column representing a different signal. Table C.1 lists the variables which each column of **yout** represent.

Table C.1: Corresponding model variables for outputs from code

Column # of yout	Variable Name in Code	Name according to Thesis Nomenclature	Significance
1	P1	$P_1(t)$	Aortic arch pressure
2	P2	$P_2(t)$	Brachiocephalic arterial pressure
3	P3	$P_3(t)$	Upper body arterial pressure
4	P4	$P_4(t)$	Upper body venous pressure
5	P5	$P_5(t)$	Superior vena cava pressure
6	P6	$P_6(t)$	Thoracic aorta pressure
7	P7	$P_7(t)$	Abdominal aorta pressure
8	P8	$P_8(t)$	Renal arterial pressure
9	P9	$P_9(t)$	Renal venous pressure
10	P10	$P_{10}(t)$	Splanchnic arterial pressure
11	P11	$P_{11}(t)$	Splanchnic venous pressure
12	P12	$P_{12}(t)$	Lower body arterial pressure
13	P13	$P_{13}(t)$	Lower body venous pressure
14	P14	$P_{14}(t)$	Abdominal venous pressure
15	P15	$P_{15}(t)$	Inferior vena cava pressure
16	Pra	$P_{ra}(t)$	Right atrial pressure
17	Pr	$P_{rv}(t)$	Right ventricular pressure
18	Ppa	$P_{pa}(t)$	Pulmonary arterial pressure
19	Ppv	$P_{pv}(t)$	Pulmonary venous pressure
20	Pla	$P_{la}(t)$	Left atrial pressure
21	P1	$P_{lv}(t)$	Left ventricular pressure
22	Qlo	$q_1(t)$	Blood flow out of left ventricle
23	Qro	$q_{pa}(t)$	Blood flow out of right ventricle
24	vspvodelt	$\Delta V_{11AB}^0(t)$	Change in splanchnic venous unstressed volume from arterial baroreflex system
25	Pe12	P_{12}^e and $P_{13}^e(t)$	Pressure external to lower body compartments
26	vupvodelt	$\Delta V_{4AB}^0(t)$	Change in upper body venous unstressed volume from arterial baroreflex system
27	vkvodelt	$\Delta V_{9AB}^0(t)$	Change in renal venous unstressed volume from arterial baroreflex system
28	vllvodelt	$\Delta V_{13AB}^0(t)$	Change in lower body venous unstressed volume from arterial baroreflex system

Continued on next page

Description of Simulink and MATLAB Code for the Cardiovascular Model

Table C.1: *continued*

Column # of yout	Variable Name in Code	Name according to Thesis Nomenclature	Significance
29	RubNew	$R_4(t)$	Upper body microvascular resistance (including reflex system contributions)
30	RrcNew	$R_9(t)$	Renal microvascular resistance (including reflex system contributions)
31	RscNew	$R_{11}(t)$	Splanchnic microvascular resistance (including reflex system contributions)
32	RlcNew	$R_{13}(t)$	Lower body microvascular resistance (including reflex system contributions)
33	vupvodeltCP	$\Delta V_4^0 \text{ CP}(t)$	Change in upper body venous unstressed volume from cardiopulmonary reflex system
34	vkvodeltCP	$\Delta V_9^0 \text{ CP}(t)$	Change in renal venous unstressed volume from cardiopulmonary reflex system
35	vspvodeltCP	$\Delta V_{11}^0 \text{ CP}(t)$	Change in splanchnic venous unstressed volume from cardiopulmonary reflex system
36	vllvodeltCP	$\Delta V_{13}^0 \text{ CP}(t)$	Change in lower body venous unstressed volume from cardiopulmonary reflex system
37	Cra	$C_{ra}(t)$	Time-varying right atrial compliance
38	Cla	$C_{la}(t)$	Time-varying left atrial compliance
39	t	—	Time from start of atrial systole
40	Crv	$C_{rv}(t)$	Time-varying right ventricular compliance
41	Clv	$C_{rl}(t)$	Time-varying left ventricular compliance
42	tv	—	Time from start of ventricular systole
43	w	$\omega(t)$	Angular velocity of centrifuge
44	Qint	$q_{\text{int}}(t)$	Fluid flow into the interstitium
45	Pth	$P_{th}(t)$	Intra-thoracic pressure
46	HR	$I(t)$	Inter-beat interval (the variable name HR is misleading)

Continued on next page

Table C.1: *continued*

Column # of yout	Variable Name in Code	Name according to Thesis Nomenclature	Significance
47	NewBeat	—	Equals 1 at time of new beat, otherwise, equals 0
48	V3a	$V_3(t)$	Upper body arterial compartmental volume (collapsible compartment)
49	V4a	$V_4(t)$	Upper body venous compartmental volume (collapsible compartment)
50	V5a	$V_5(t)$	Superior vena cava compartmental volume (collapsible compartment)
51	V9a	$V_9(t)$	Renal venous compartmental volume (collapsible compartment)
52	V11a	$V_{11}(t)$	Splanchnic venous compartmental volume (collapsible compartment)
53	V14a	$V_{14}(t)$	Abdominal venous compartmental volume (collapsible compartment)
54	Vlva	$V_{11}(t)$	Left Ventricular compartmental volume
55	Vint	$V_{\text{int}}(t)$	Interstitial volume (from volume loss)
56	Q5i	$q_5(t)$	Blood flow into superior vena cava
57	Q5o	$q_{5,\text{out}}(t)$	Blood flow out of superior vena cava
58	Q5i	$q_{15}(t)$	Blood flow into inferior vena cava

Post-simulation, m-file code is run to derive other important variables from the output data, namely, compartmental and total volumes, total peripheral resistance, MAP, SAP, DAP, heart rate, cardiac output, and total volume in the legs. The code for computing these variables from the simulation output (as given in the model in Figure C.2 and Table C.1) is reproduced below.

```
%initcond contains the nominal parameters of the model.
u=initcond;
%initialize parameters
T=u(1)/1000;
Cls=u(2);
```

Description of Simulink and MATLAB Code for the Cardiovascular Model

```
Cld=u(3);  
Crs=u(4);  
Crd=u(5);  
R1=u(6);  
R2=u(7);  
R3=u(8);  
R4=u(9);  
R5=u(10);  
R6=u(11);  
R7=u(12);  
R8=u(13);  
R9=u(14);  
R10=u(15);  
R11=u(16);  
R12=u(17);  
R13=u(18);  
R14=u(19);  
R15=u(20);  
Rub=u(21);  
Rrc=u(22);  
Rsc=u(23);  
Rlc=u(24);  
Rro=u(25);  
Rpv=u(26);  
Rli=u(27);  
Vt=u(28);  
Vo=u(29);  
C1=u(30);  
C2=u(31);  
C3=u(32);  
C4=u(33);  
C5=u(34);  
C6=u(35);  
C7=u(36);  
C8=u(37);  
C9=u(38);  
C10=u(39);  
C11=u(40);  
C12=u(41);  
C13=u(42);  
C14=u(43);  
C15=u(44);  
Cpa=u(45);  
Cpv=u(46);
```

```
Pth0=u(47);
Pe=u(48);
Ph1=u(49);
Ph2=u(50);
Ph3=u(51);
Ph4=u(52);
Ph5=u(53);
Ph6=u(54);
Ph7=u(55);
Ph8=u(56);
Ph9=u(57);
Ph10=u(58);
Ph11=u(59);
Ph12=u(60);
Ph13=u(61);
Ph14=u(62);
Ph15=u(63);
R0=u(64);
Clad=u(65);
Clas=u(66);
Crad=u(67);
Crass=u(68);
Tsla=u(69);
Tav=u(70);
R_tri=u(71);
R_mitral=u(72);
Tslv=u(73);
Vmaxsp=u(74);
Vmaxll=u(75);
Vmaxab=u(76);

Ts = (1/3)*sqrt(T);
Td = T-Ts-Ts/2;

%read output data
P1=yout(:,1);
P2=yout(:,2);
P3=yout(:,3);
P4=yout(:,4);
P5=yout(:,5);
P6=yout(:,6);
P7=yout(:,7);
P8=yout(:,8);
P9=yout(:,9);
```

Description of Simulink and MATLAB Code for the Cardiovascular Model

```
P10=yout(:,10);
P11=yout(:,11);
P12=yout(:,12);
P13=yout(:,13);
P14=yout(:,14);
P15=yout(:,15);
Pra=yout(:,16);
Prv=yout(:,17);
Ppa=yout(:,18);
Ppv=yout(:,19);
Pla=yout(:,20);
Plv=yout(:,21);

Cla=yout(:,38);
Clv=yout(:,41);
Cra=yout(:,37);
Crv=yout(:,40);

Pth=yout(:,45);
PeLB=yout(:,25);

upV0delt=yout(:,26);
upV0deltCP=yout(:,33);
kV0delt=yout(:,27);
kV0deltCP=yout(:,34);
spV0delt=yout(:,24);
spV0deltCP=yout(:,35);
l1V0delt=yout(:,28);
l1V0deltCP=yout(:,36);

%set unstressed volumes
ZV1=21+zeros(length(tout),1);
ZV2=5+zeros(length(tout),1);
ZV3=200+zeros(length(tout),1);
ZV4n=645;
ZV4=ZV4n+upV0delt+upV0deltCP;
ZV5=16+zeros(length(tout),1);
ZV6=16+zeros(length(tout),1);
ZV7=10+zeros(length(tout),1);
ZV8=20+zeros(length(tout),1);
ZV9n=30;
ZV9=ZV9n+kV0delt+kV0deltCP;
for n123=1:length(ZV9)
    if ZV9(n123)<5
```

```

ZV9(n123)=5;
end
end
ZV10=300+zeros(length(tout),1);
ZV11n=1146;
ZV11=ZV11n+spV0delt+spV0deltCP;
ZV12=200+zeros(length(tout),1);
ZV13n=716;
ZV13=ZV13n+l1V0delt+l1V0deltCP;
ZV14=79+zeros(length(tout),1);
ZV15=33+zeros(length(tout),1);
ZVra=14+zeros(length(tout),1);
ZVrv=46+zeros(length(tout),1);
ZVpa=160+zeros(length(tout),1);
ZVpv=430+zeros(length(tout),1);
ZVla=24+zeros(length(tout),1);
ZVlv=55+zeros(length(tout),1);

%Compute compartmental volumes
V1=C1*(P1-Pth)+ZV1;
V2=C2*(P2-Pth)+ZV2;
V3=yout(:,48);
V4=yout(:,49);
V5=yout(:,50);
V6=C6*(P6-Pth)+ZV6;
V7=C7*(P7-Pe)+ZV7;
V8=C8*(P8-Pe)+ZV8;
V9=yout(:,51);
V10=C10*(P10-Pe)+ZV10;
V11=yout(:,52);
V12=C12*(P12-PeLB)+ZV12;
V13=2*Vmax11/pi*atan(pi*C13*(P13-PeLB)/(2*Vmax11))+ZV13;
V14=yout(:,53);
V15=C15*(P15-Pth)+ZV15;
Vra=Cra.* (Pra-Pth)+ZVra;
Vrv=CrV.* (Prv-Pth)+ZVrv;
Vpa=Cpa*(Ppa-Pth)+ZVpa;
Vpv=Cpv*(Ppv-Pth)+ZVpv;
Vla=Cla.* (Pla-Pth)+ZVla;
Vlv=yout(:,54);
Vint=yout(:,55);

%Compute total unstressed volume and total volume

```

Description of Simulink and MATLAB Code for the Cardiovascular Model

```
ZVtot=ZV1+ZV2+ZV3+ZV4+ZV5+ZV6+ZV7+ZV8+ZV9+ZV10+ZV11...
+ZV12+ZV13+ZV14+ZV15+ZVra+ZVrv+ZVpa+ZVpv+ZVla+ZVlv;

Vtot=V1+V2+V3+V4+V5+V6+V7+V8+V9+V10+V11...
+V12+V13+V14+V15+Vra+Vrv+Vpa+Vpv+Vla+Vlv+Vint;

%read TPR data
Rubn=yout(:,29);
Rrcn=yout(:,30);
Rscn=yout(:,31);
Rlcn=yout(:,32);

Rtot=1./(1./Rubn+1./Rrcn+1./Rscn+1./Rlcn);
figure;plot(tout,Rtot)
title('Total Peripheral Resistance')

%HR

HR=60./(yout(:,46));
figure;plot(tout,HR)
title('Heart Rate')

%Venous ZPFV

TotVenousZPFV= ZV4+ZV9+ZV11+ZV13;
figure;plot(tout,TotVenousZPFV)
title('Total Venous Zero-Pressure Filling Volume')

%Total Leg Volume

TotalLegVol=V12+V13;
figure;plot(tout,TotalLegVol)
title('Total Volume in Legs')

%Total Abdominal Volume

TotalAbVol=V7+V8+V9+V10+V11+V14;
figure;plot(tout,TotalAbVol)
title('Total Volume in Abdomen')

%compute orthostatic stress inputs
ww=yout(:,43);
```

```

Ph13=0.0007501*ww.^2*0.5*((55+(161-55)/3)^2-55^2);
Ph11=0.0007501*ww.^2*0.5*((55+(65-55)/2)^2-55^2);
Ph14=0.0007501*ww.^2*0.5*((40.5+(55-40.5)/2)^2-40.5^2);

%compute fraction of volume lost to interstitium that was from legs.
Phtotal=Ph13+Ph11+Ph14;
Phtotal(find(Phtotal==0))=1;
VintLeg=(Ph13./Phtotal).*Vint;

%take beat-to-beat averaged values by approximating the integral over one
%beat and dividing by the time length of the beat.

step=diff(tout);

NewBeat=yout(:,47);
vec=find(NewBeat==1); %vec now holds starting 'sample numbers' of each beat.

for i=1:length(vec)-1
    st=vec(i);
    en=vec(i+1);
    %MAP
    MAP(i)=sum(P1(st:en-1).*step(st:en-1))/(tout(en)-tout(st));
    %DAP
    DAP(i)=min(P1(st:en-1));
    %SAP
    SAP(i)=max(P1(st:en-1));
    %Average Transmural Right-Atrial Pressure
    dPra=Pra-Pth;
    AvgDPra(i)=sum(dPra(st:en-1).*step(st:en-1))/(tout(en)-tout(st));
    %CO
    qlvo=yout(:,22);
    CO(i)=sum(qlvo(st:en-1).*step(st:en-1))/(tout(en)-tout(st));
    %Average Total Leg Volume
    AvgTotalLegVol(i)=sum(TotalLegVol(st:en-1).*step(st:en-1))/(tout(en)-tout(st));
    %Average Total Ab Volume
    AvgTotalAbVol(i)=sum(TotalAbVol(st:en-1).*step(st:en-1))/(tout(en)-tout(st));
    %Average Compartmental Volumes
    AvgV1(i)=sum(V1(st:en-1).*step(st:en-1))/(tout(en)-tout(st));
    AvgV2(i)=sum(V2(st:en-1).*step(st:en-1))/(tout(en)-tout(st));
    AvgV3(i)=sum(V3(st:en-1).*step(st:en-1))/(tout(en)-tout(st));
    AvgV4(i)=sum(V4(st:en-1).*step(st:en-1))/(tout(en)-tout(st));
    AvgV5(i)=sum(V5(st:en-1).*step(st:en-1))/(tout(en)-tout(st));
    AvgV6(i)=sum(V6(st:en-1).*step(st:en-1))/(tout(en)-tout(st));
    AvgV7(i)=sum(V7(st:en-1).*step(st:en-1))/(tout(en)-tout(st));

```

Description of Simulink and MATLAB Code for the Cardiovascular Model

```
AvgV8(i)=sum(V8(st:en-1).*step(st:en-1))/(tout(en)-tout(st));
AvgV9(i)=sum(V9(st:en-1).*step(st:en-1))/(tout(en)-tout(st));
AvgV10(i)=sum(V10(st:en-1).*step(st:en-1))/(tout(en)-tout(st));
AvgV11(i)=sum(V11(st:en-1).*step(st:en-1))/(tout(en)-tout(st));
AvgV12(i)=sum(V12(st:en-1).*step(st:en-1))/(tout(en)-tout(st));
AvgV13(i)=sum(V13(st:en-1).*step(st:en-1))/(tout(en)-tout(st));
AvgV14(i)=sum(V14(st:en-1).*step(st:en-1))/(tout(en)-tout(st));
AvgV15(i)=sum(V15(st:en-1).*step(st:en-1))/(tout(en)-tout(st));
AvgVra(i)=sum(Vra(st:en-1).*step(st:en-1))/(tout(en)-tout(st));
AvgVrv(i)=sum(Vrv(st:en-1).*step(st:en-1))/(tout(en)-tout(st));
AvgVpa(i)=sum(Vpa(st:en-1).*step(st:en-1))/(tout(en)-tout(st));
AvgVpv(i)=sum(Vpv(st:en-1).*step(st:en-1))/(tout(en)-tout(st));
AvgVla(i)=sum(Vla(st:en-1).*step(st:en-1))/(tout(en)-tout(st));
AvgVlv(i)=sum(Vlv(st:en-1).*step(st:en-1))/(tout(en)-tout(st));
%Average total volume
AvgVtot(i)=sum(Vtot(st:en-1).*step(st:en-1))/(tout(en)-tout(st));
%Average volume lost to interstitium
AvgVint(i)=sum(Vint(st:en-1).*step(st:en-1))/(tout(en)-tout(st));
%average volume from legs lost to interstitium
AvgVintLeg(i)=sum(VintLeg(st:en-1).*step(st:en-1))/(tout(en)-tout(st));
times(i)=(tout(st)+tout(en))/2;
end
```

Appendix D

Data Processing Code

As discussed in Section 4.1, we detected the peak times from the ECG data using a modified version of an algorithm employed by Hastreiter [39]. The algorithm first filters the ECG data and subsequently records the peak times of the filtered data. The MATLAB code for this algorithm is given below.

```
%y contains data
%initialize variables
w=y(:,5)*5;      %angular velocity
ABP=y(:,4)*100;  %Arterial Blood Pressure
SG1=y(:,14);     %Strain Gauge data (four signals)
SG2=y(:,15);
SG3=y(:,16);
SG4=y(:,17);
ECG1=y(:,2);     %ECG Data

sr=1000;    %sample rate
min2=length(ECG1)/sr/60; %number of minutes in data

%plot first 10 seconds of ECG data
xo=ECG1(1:10*1000);
figure; subplot(221), plot(t(1:10*1000),xo)
title('First Ten seconds of ECG signal')
xlabel('Time (s)')
ylabel('Voltage (V)')

%Take FFT of ECG data and plot
fre=[1/4096:1/4096:1]*sr;
xfft=abs(fft(xo,4096));
subplot(222), plot(fre,xfft)
axis([0 75 0 800])
title('FFT')
xlabel('Frequency (Hz)')
```

Data Processing Code

```
%matched filtering of ECG data
fmin=10; fmax=30; order=100; wn=[fmin*2/sr fmax*2/sr];
B=fir1(order,wn); J=fftfilt(B,ECG1);

%plot filtered data
subplot(223), plot(t(1:10*sr),J(1:10*sr));
xlabel('Time (s)')
ylabel('Voltage (V)')

%Take FFT of the filtered data and plot
Y=abs(fft(J(1:10*sr),4096));
subplot(224),plot(fre,Y)
axis([0 75 0 800])
title('FFT of Filtered Data')
xlabel('Frequency (Hz)')

k=1;
peaktime=zeros(1,min2*100);
r=-1000;
%J is filtered ECG data
for i=1:length(J)
    %first find local max in data over the last 5 seconds
    if i > 5*sr
        m=max(J(i-5*sr:i));
    else
        m=max(J(sr*0.1:5*sr));
    end
    if i>0.1*sr
        %mark a 'peak' at current time if value > 0.7*(local max)
        %AND if a period of 0.45 s has elapsed since the last peaktime
        if (((J(i))> .7*m) & ((i-r) > 0.45*sr))
            peaktime(k)=t(i);
            k=k+1;
            r=i;
        end
    end
end
peaktime=peaktime(1:k-1);
```

The following code computes HR, MAP, SAP, DAP, mean strain gauge impedance, and mean angular velocity for each beat. It is necessary to average strain gauge impedance and angular velocity over one beat so that these signals can be compared to HR, MAP,

SAP, and DAP on the same time scale.

```
rr=diff(peaktme);
hr=60./rr;
%this code uses the peak times to find
%MAP,SAP,DAP, mean angular velocity,
%and mean strain gauge impedance
%for each beat
startind=1; for k=1:length(peaktme)
    endind=find(abs(t-peaktme(k))<0.0005);
    mw(k)=mean(w(startind:endind-1)); %mean angular velocity
    MAP(k)=mean(ABP(startind:endind-1));
    SAP(k)=max(ABP(startind:endind-1));
    DAP(k)=min(ABP(startind:endind-1));
    mSG1(k)=mean(SG1(startind:endind-1)); %the four strain gauge signals
    mSG2(k)=mean(SG2(startind:endind-1));
    mSG3(k)=mean(SG3(startind:endind-1));
    mSG4(k)=mean(SG4(startind:endind-1));
    startind=endind;
end
```


Bibliography

- [1] T. Davis. *Teaching Physiology Through Interactive Simulation of Hemodynamics*. Master's thesis, Department of Electrical Engineering and Computer Science, Massachusetts Institute of Technology, Cambridge, MA, February 1991.
- [2] T. Heldt. *Computational Models of Cardiovascular Response to Orthostatic Stress*. PhD thesis, Harvard-MIT Division of Health Sciences and Technology, Massachusetts Institute of Technology, Cambridge, MA, September 2004
- [3] O. Frank. Die Grundform des arterielen Pulses Erste Abhandlung: mathematische Analyse. *Z. f. Biol.*, 37:483-526, 1899.
- [4] V.K. Sud, R. Srinivasan, J.B. Charles, and M.W. Bungo. Effects of lower-body negative pressure on blood flow with applications to the human cardiovascular system. *Medical & Biological Engineering & Computing*, 31(6):569-575, 1993.
- [5] F.M. Melchior, R.S. Srinivasan, P.H. Thullier, and J.M. Clre. Simulation of cardiovascular response to lower body negative pressure from 0 to -40 mmHg. *Journal of Applied Physiology*, 77(2):630-640, 1994.
- [6] D. Jaron, T.W. Moore, and J. Bai. Cardiovascular response to acceleration stress: a computer simulation. *Proceedings of the IEEE*, 76(6):700-707, 1988.
- [7] J.F. Green and N.C. Miller. A model describing the response of the circulatory system to acceleration stress. *Annals of Biomedical Engineering*, 1(4):455-467, 1973.
- [8] D.J. Pancratz, J.B. Bomar, Jr. and J.H. Raddin, Jr. Modeling platform dynamics and physiological response to short arm centrifugation. AL/CF-TR-1994-0025. NASA report N95-20457, 1995.
- [9] L.R. Young, H. Hecht, L.E. Lyne, K.H. Sienko, C.C. Cheung, and J. Kavelaars. Artificial gravity head movements during short-radius centrifugation. *Acta Astronautica* 49:215-226, 2001.
- [10] Z. Samar. *Cardiovascular Parameter Estimation using a Computational Model*. SM thesis, Department of Electrical Engineering and Computer Science, Massachusetts Institute of Technology, Cambridge, MA, May 2005
- [11] A.A. Pollack and E. H. Wood. Venous pressure in the saphenous vein at the ankle in man during exercise and changes in posture. *Journal of Applied Physiology*, 1:649-662, 1949.

BIBLIOGRAPHY

- [12] D.J. Griffiths. Principles of blood flow through collapsible tubes. In A.M.N. Gardner and R.H. Fox, editors, *The return of blood to the heart: venous pumps in health and disease*, pages 159-170. John Libbey & Company Ltd., London, 1993.
- [13] H. Senzaki, C. Chen, and D.A. Kass. Single-beat estimation of end-systolic pressure-volume relations in humans. *Circulation*, 94(10):2497-2506, 1996.
- [14] B.W. Hyndman and R.K. Mohn. A model of the cardiac pacemaker and its use in decoding the information content of cardiac intervals. *Automedica*, 1:239-252, 1975.
- [15] R.W. de Boer, J.M. Karemaker, and J. Stracke. Description of heart rate variability data in accordance with a physiological model of the genesis of heartbeats. *Psychophysiology*, 22(2):147-155, 1985.
- [16] J. Mead and E.A. Gaensler. Esophageal and pleural pressures in man, upright and supine. *Journal of Applied Physiology*, 14(1):81-83, 1959.
- [17] B.G. Gerris, Jr., J. Mead, and N.R. Frank. Effect of body position on esophageal pressure and measurement of pulmonary compliance. *Journal of Applied Physiology*, 14(4):521-524, 1959.
- [18] J. Lundvall, P. Bjerkhoel, S. Quittenbaum, and P. Lindgren. Rapid plasma volume decline upon quiet standing reflects large filtration capacity in dependent limbs. *Acta Physiologica Scandinavica*, 158(2):161-167, 1996.
- [19] R.C. Tarazi, H.J. Melsher, H.P. Dustan, and E.D. Frohlich. Plasma volume changes with upright tilt: studies in hypertension and in syncope. *Journal of Applied Physiology*, 28(2):121-126, 1970.
- [20] H. Hinghofer-Szalkay and M. Moser. Fluid and protein shifts after postural changes in humans. *American Journal of Physiology*, 250(19):H68-H75, 1986.
- [21] G. Jacob, A.C. Ertl, J.R. Shannon, R. Furlan, R.M. Robertson, and D. Robertson. Effect of standing on neurohumoral responses and plasma volume in healthy subjects. *Journal of Applied Physiology*, 84(3):914-921, 1998.
- [22] R.D. Hagan, F.J. Diaz, and S.M. Horvath. Plasma volume changes with movement to the upright position. *Journal of Applied Physiology*, 45(3):414-417, 1978.
- [23] J. Lundvall and P. Bjerkhoel. Failure of hemoconcentration during standing to reveal plasma volume decline induced in the erect posture. *Journal of Applied Physiology*, 77(5):2155-2162, 1994.
- [24] P. Bjerkhoel and J. Lundvall. Rapid and large plasma volume decrease upon short-term quiet standing. *Acta Physiologica Scandinavica*, 150(3):347-348, 1994.
- [25] P. Bjerkhoel and J. Lundvall. Pronounced plasma fluid loss into dependent regions on standing. *Acta Physiologica Scandinavica*, 150(3):347-348, 1994.

BIBLIOGRAPHY

- [26] J. Lundvall and P. Bjerkhoel. Pronounced and rapid plasma volume reduction upon quite standing as revealed by a novel approach to the determination of the intravascular volume change. *Acta Physiologica Scandinavica*, 154(2):131-142, 1995.
- [27] J. Lundvall and P. Lindgren. F-cell shift and protein loss strongly affect validity of PV reductions indicated by Hb/Hct and plasma proteins. *Journal of Applied Physiology*, 84(3):822-829, 1998.
- [28] J. Lundvall, P. Bjerkhoel, C. Ivarsson, and T. Länne. Dynamics of transcapillary fluid transfer and plasma volume during lower body negative pressure. *Acta Physiologica Scandinavica*, 147(2):163-172, 1993.
- [29] M. Aratow, S.M. Fortney, D.E. Watenpaugh, A.G. Crenshaw, and A.R. Hargens. TRanscapillary fluid responses to lower body negative pressure. *Journal of Applied Physiology*, 74(6):2763-2770, 1993.
- [30] H.W. Ryder, W.E. Molle, and E.B. Ferris, Jr. The influence of the collapsibility of veins on venous pressure, including a new procedure for measuring tissue pressures. *Journal of Clinical Investigation*, 23(3):333-342, 1943.
- [31] F.P. Knowlton and E.H. Starling. The influence of variations in temperature and blood pressure on the performance of the isolated mammalian heart. *Journal of Physiology*, 44(3):206-209, 1912.
- [32] R.W. Brower and A. Noordergraaf. Pressure flow characteristics of collapsible tubes: A reconciliation of seemingly contradictory results. *Annals of Bioengineering*, 1(3):333-335, 1973.
- [33] S. Permutt and R.L. Riley. Hemodynamics of collapsible vessels with tone: the vascular waterfall. *Journal of Applied Physiology*, 18(5), 1963.
- [34] A. Shapiro. Steady flow in collapsible tubes. *Journal of Biomechanical Engineering*, 99:126-147, 1977.
- [35] R.D. Kamm. Flow through collapsible tubes. In R. Skalak and S. Chien, editors, *Handbook of Bioengineering*, chapter 23, pages 23.1-23.19. McGraw-Hill, New York, 1987.
- [36] R.W. deBoer, J.M. Karemaker, and J. Stackee. Hemodynamic fluctuations and baroreflex sensitivity in humans: A beat-to-beat model. *American Journal of Physiology - Heart and Circulatory Physiology*, 253(22):H680-H689, 1987.
- [37] G. Mancia and A.L. Mark. Arterial baroreflex in humans. In T.J. Shepard, J.M. Aboud, and S.R. Geiger, editors, *The peripheral circulation*, volume III (Part 2) of *Handbook of Physiology, Section 2: The Cardiovascular System*, chapter 20, pages 755-793. American Physiological Society, Bethesda, MD, 1983.
- [38] R. Mukkamala. *A Forward Model-Based Analysis of Cardiovascular System Identification Methods*. PhD thesis, Department of Electrical Engineering and Computer Science, Massachusetts Institute of Technology, Cambridge, MA, June 2000.

BIBLIOGRAPHY

- [39] D. Hastreiter. *Artificial Gravity as a Countermeasure to Spaceflight Deconditioning: The Cardiovascular Response to a Force Gradient*. SM thesis, Department of Aeronautics and Astronautics, Massachusetts Institute of Technology, Cambridge, MA, June 1997.
- [40] K. van Heusden, J. Gisolf, W.J. Stok, S. Dijkstra and J.M. Karemaker. Mathematical modeling of gravitational effects on the circulation: importance of the time course of venous pooling and blood volume changes in the lungs. *American Journal of Physiology - Heart and Circulatory Physiology*, 291:2152-2165, 2006.
- [41] M. Kleiber. Body size and metabolism. *Hilgardia*, 6:315-353, 1932.
- [42] T. McMahon. Size and shape in biology. *Science*, 179(79):1201-1204, 1973.
- [43] T.A. McMahon. Scaling physiological time. *Lectures in Mathematics in the Life Sciences*, 13:131-163, 1980.